

Review

A Systematic Review on the Synthesis of Silicon Carbide: An Alternative Approach to Valorisation of Residual Municipal Solid Waste

Adhithiya Venkatachalapati Thulasiraman  and Mahesh Ganesapillai * 

Mass Transfer Group, School of Chemical Engineering, Vellore Institute of Technology, Vellore 632014, India

* Correspondence: maheshpillai@vit.ac.in; Tel.: +91-9790299447

Abstract: Over the past several decades, industrialised and developing nations have attempted to enhance sustainability. Demands for energy and the acceleration in environmental deterioration are the two primary obstacles to progress. The daily generation of municipal solid waste has been a significant factor in the deterioration of the ecology. To address this issue, a considerable amount of municipal solid waste may be used to synthesise SiC nanomaterials from organic and inorganic fractions and use them as carbon and silica sources. Nanomaterials have progressively received widespread prominence as the development of particulate materials accelerates at an incredible rate. One such material is silicon carbide (SiC), which has garnered considerable interest due to its remarkable performance and wide variety of applications. This review article discusses the SiC polytypes, including cubic, hexagonal, and rhombohedral SiC. The characteristics of silicon carbide, such as its biomimetic, surface, and thermal properties, are also discussed. In addition, the synthesis of silicon carbide was described in depth, including microwave sintering, the calcination method, the carbothermal redox reaction, and much more. The final section describes the applications of silicon carbide, including wastewater treatment, medical implants, and gas detection.

Keywords: nanomaterials; polytypes; wastewater treatment; biomedical properties



Citation: Thulasiraman, A.V.; Ganesapillai, M. A Systematic Review on the Synthesis of Silicon Carbide: An Alternative Approach to Valorisation of Residual Municipal Solid Waste. *Processes* **2023**, *11*, 283. <https://doi.org/10.3390/pr11010283>

Academic Editor: Elsayed Elbeshbishy

Received: 16 December 2022

Revised: 8 January 2023

Accepted: 10 January 2023

Published: 15 January 2023



Copyright: © 2023 by the authors. Licensee MDPI, Basel, Switzerland. This article is an open access article distributed under the terms and conditions of the Creative Commons Attribution (CC BY) license (<https://creativecommons.org/licenses/by/4.0/>).

1. Introduction

Municipal solid waste (MSW) originates from households, institutions, construction and demolition sites, and other sources. The World Bank predicts that global MSW generation will reach 2.2 billion tonnes by 2025 [1]. Waste management has become a global threat due to new technology, affecting both developed and developing countries. Poor waste management has ecological, social, and economic impacts. Management of MSW in an environmentally responsible way is essential for balancing the three pillars of sustainability and reducing negative social and economic impacts. Separating MSW into organic (carbon-rich) and inorganic (silica-rich) waste fractions would allow it to be used as a raw material in synthesising SiC, which could subsequently be used to help reduce MSW. Biomass is the organic fraction of MSW that cannot be consumed or converted into a product. Biomass waste includes corn stover, sugarcane bagasse, animal manure, sawdust, and wood shavings. These substances contain carbohydrates; lipids; proteins; lignin; and minerals like calcium, iron, and phosphorus. Usually, waste is either burned or dumped without sorting. Combustion emits methane, carbon monoxide, and nitrogen dioxide, making it environmentally harmful.

In 2009, a Swedish study revealed that the primary cause of the brown haze that blanketed significant hectares of South Asia was mainly the incineration of biomass compared with fossil fuel combustion. Hence, it is worthwhile to consider transforming waste into something valuable to achieve a sustainable waste management system. The researchers synthesised SiC (50–100 nm in diameter and $64.21 \text{ m}^2 \cdot \text{g}^{-1}$) using automotive waste glass (rich in silica) and waste coffee grounds (rich in carbon) [2]. SiC inherits the distinctive

qualities of composite structural materials, such as strength, hardness, corrosion resistance, and wear resistance. SiC can be used as feedstock in abrasives and modern refractories due to its high-temperature characteristics, including a low thermal expansion coefficient, oxidation resistance, and high thermal conductivity. SiC's high critical breakdown voltage and rapid carrier saturation drift velocity make it a possible third-generation semiconductor for high-frequency applications. Three-dimensional objects known as nanomaterials have one or more dimensions in the nanometre range (1–100 nm). The size effect refers to a phenomenon where a material's qualities change as its size reduces. The effect is substantial for nanoscale particles in three dimensions because there is a negative relationship between the number of atoms and the separation between energy levels. The move from macroscopic progression to distinct microscopic atoms, known as "quantum" functionalities, widens the energy gap of the substance [3]. Each particle has fewer atoms, and the surface atoms are unstable, leading to a high surface energy and a lower melting point.

Other features of nanoparticles, such as magnetic, optical, and thermal properties, may change significantly more than bulk materials. Initially, the SiC nanoparticle was first discovered by Acheson et al. [4] by using silica and carbon as feedstock. In addition to this, SiC nanoparticles have gained attention due to their "quantum" properties and exceptional attributes, and articles on their generation and applications are increasing [5]. Their applications include the aircraft industry, the automobile and transportation industry, and spacecraft and power distribution systems. Electronics and sensors are critical for improving system capabilities and efficiency in the aircraft sector. Some of these devices are in the aircraft's aero surface portions as well as in hot engines to manage their key components, where reliable and stable operation under high-temperature circumstances is required. SiC devices can reduce a significant proportion of wiring and avoid problems related to the cooling system [6].

High-temperature SiC electronics could remove the requirement for thermal radiators in spaceship systems. These radiators are required when low-temperature electronics are used to dissipate the heat generated by the spacecraft's electronics. In the case of the low option, the use of SiC electronics will reduce the size of the radiator, whereas the high option may eliminate the cooling system. Consequently, the satellite's load would be reduced. This is essential because the extra space and weight saved will allow us to fit vital equipment on a satellite.

The long-term performance of solar system exploration instruments necessitates SiC electronics; for example, the parching atmosphere of Venus's surface at 460 °C requires high-temperature electronics [7]. With SiC power electronics, electric power distribution systems can be enhanced. In modern power electronics, a significant excess power reserve is created to provide a safety margin for the electric power supply, allowing it to satisfy power demand in normal and emergency situations. Using SiC power electronics that can recognise and compensate for local errors in real-time can lower this margin. It eliminates the requirement for additional power plants. These devices with existing powerlines will increase power transmission capacity [8]. All these applications motivate scientists to conduct research in the field of SiC.

Over the past two decades, researchers have authored review articles on the structure, characteristics, and applications of silicon carbide (Elsevier search engine: as of 26 July 2022. Figure 1).

Although researchers have conducted an extensive study on the synthesis, characteristics, and characterisation of SiC, to our knowledge, the synthesis of SiC from municipal solid waste is limited. As a result, this review is structured as follows: The first section focuses on the polytypes of SiC, followed by the various methods for synthesising SiC, such as carbothermal redox reaction, microwave sintering, pyrolysis, and detonation. Furthermore, the article discusses the biomimetic, surface, electrical, and other properties of SiC. Lastly, the article details the applications of SiC that include energy-based, composite-based, and medical fields.

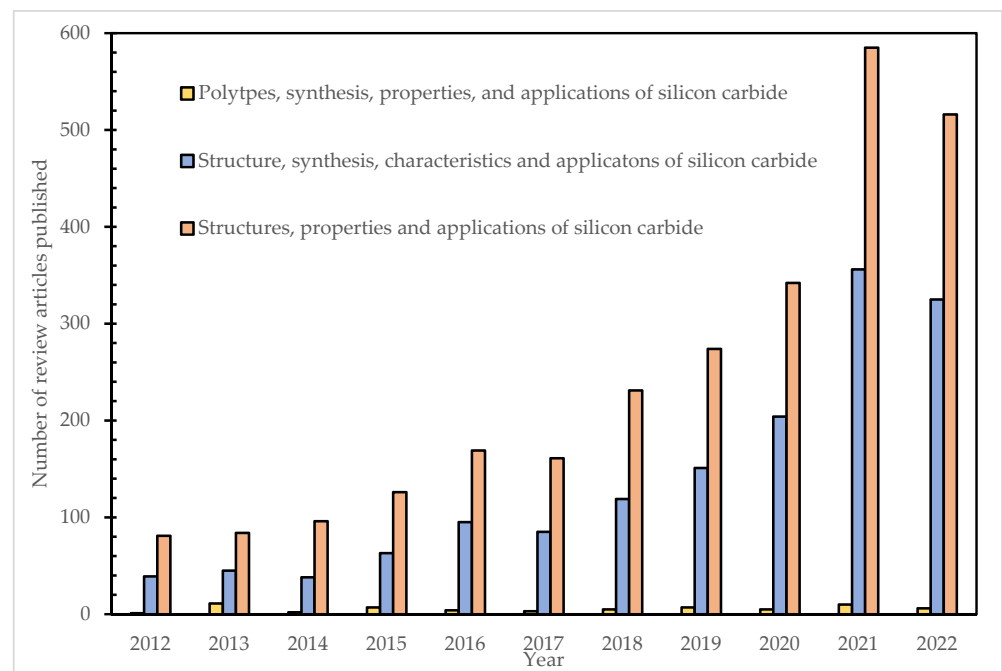


Figure 1. Number of review articles published per year from 2012 to 2022.

This article aims to establish a bridge for researchers working on artificial neural networks and HYSYS software to use the process parameters available in the synthesis of SiC so that they can build a model that may have the ability to determine the ideal process parameter that could generate a significant amount of SiC from the waste that is generated every day in an inexpensive and environmentally friendly manner.

2. Structure of Silicon Carbide

SiC crystallisation was discovered as early as the 1900s. Polytypism is a significant crystalloid–chemical phenomenon for viewing crystalline substances as interconnected elements of integrated frameworks, as well as a cognition technique helpful in solving fundamental and empirical problems. Carborundum, or silicon carbide, is composed of interlocking sheets of silicon and carbon covalently bound together. In Figure 2, a tetravalent element (carbon) is connected to a semiconductor substance (silicon), where the closest interconnected material is 1.94 Å in length. In comparison, the closest span between two components of the same compound in the SiC lattice is 3.10 Å in length.

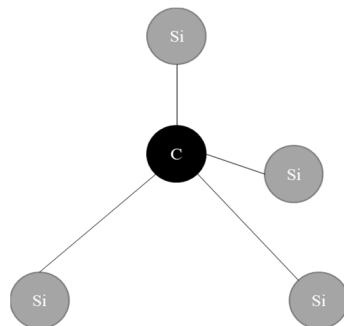


Figure 2. Covalent bonding of silicon carbide.

They are usually in the form of SiC_4 or CSi_4 , as represented. Pauling's equation was used to calculate the 12% ionic contribution of neighbourhood-oriented tetra-bonds. The modest positive charge on the Si atom causes the ionic contribution to the bonds between atoms. This is evident in the SiC X-ray spectrometer's Ka doublet transfer. SiC's

polymorphism means that it has several distinct 1D ordering patterns with no change in stoichiometry.

Even though there are numerous SiC polytypes, it is usual to refer to 3C-SiC as β -SiC and any non-cubic structures (4H-SiC, 6H-SiC, 9R-SiC, and 15R-SiC) as α -SiC. The stacking sequence distinguishes polytypes [9]. α -SiC is heated more than β -SiC. 4H-SiC, 6H-SiC, and 15R-SiC stack ABCB..., ABCACB..., and ABCABCBCABACBCB..., as represented in Figure 3. The Si/C atomic ratio is normally one; however, vacancies can change it. Table 1 shows SiC polytypes' lattice constants, electron mobility, bandgap, and more. The difference in bulk energy between SiC polytypes is $0.99 \text{ meV}\cdot\text{atom}^{-1}$, according to abinitio calculations. Nishino et al. [10] developed an efficient approach to synthesise 3C-SiC on silicon; many groups have gathered data on its development mechanisms, setting the groundwork for its widespread use. Cubic-SiC or 3C-SiC is the only substance produced on a host substrate, with the advantage of growing the SiC at the necessary thickness for the intended application. The potential to grow SiC on the silicon wafer substrate with a diameter of 150 nm has been a boon for scaling up.

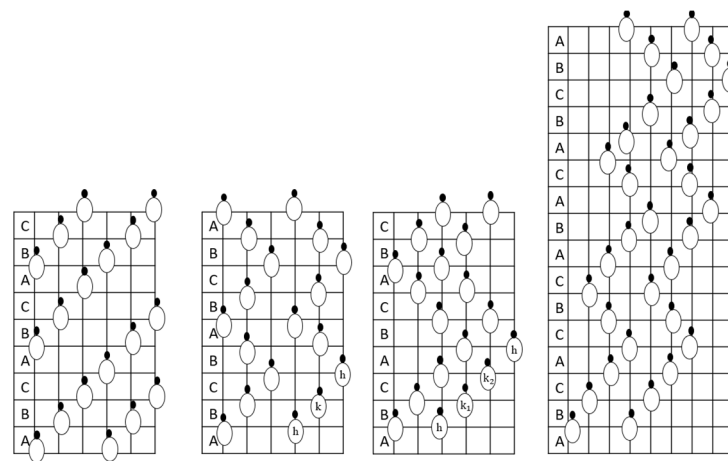


Figure 3. Structure of both alpha and beta silicon carbide.

Table 1. Characteristics of cubic and hexagonal silicon carbide.

Properties	Unit/Condition	Types of Silicon Carbide				References
		Cubic	Hexagonal			
		3C	2H	4H	6H	
Bandgap	eV	2.360	3.300	3.263	3.023	[11]
Lattice constant a	Å	3.083	3.076	3.070–3.081	3.081	
Lattice constant c	Å	7.551	5.048	10.05–10.08	15.117	
Lattice constant c/na	-	0.817	0.821	-	0.818	
Si/C	-	1.046	-	1.001	1.022	
Carbon vacancies	10^{20} cm^{-3}	33.6	-	7.3	16.3	
Jagodzinskii notation		h	hc	hcc	c	[12]
Critical breakdown field strength	$\text{MV}\cdot\text{cm}^{-1}$	>1.5	-	2–3	2–3	
Saturation rate	$10^7 \text{ cm}\cdot\text{s}^{-1}$	2.7	-	2	2	
Dielectric constant	Static	9.72	-	9.66	9.66	
	High Frequency	6.52	-	6.52	6.70	
Infrared refractive index		2.55	-	2.55–2.59	2.55–2.59	
Optical photon energy	meV	102.8	-	104.2	104.2	[13]
Radiant recombinant coefficient	$10^{-12} \text{ cm}^3\cdot\text{s}^{-1}$	-	-	1.5	-	
Phonon Energy	meV	-	-	46.7–104.3	36.3–104.7	
Space group	-	F43m	P6 ₃ mc	P6 ₃ mc	P6 ₃ mc	
Hexagonality	%	0	100	50	33	
Density	$\text{g}\cdot\text{cm}^{-3}$	3.215	3.219	3.215	3.212	
Thermal conductivity	$\text{W}\cdot\text{cm}^{-1}\text{k}^{-1}$	3.6	-	4.9	4.9	[14]
Electron Mobility	$\text{cm}^2\cdot\text{V}^{-1}\text{s}$ 30 °C	≤1000	-	≤850	≤450	
Hole Mobility	$\text{cm}^2\cdot\text{V}^{-1}\text{s}$ 30 °C	≤40	-	≤120	≤100	
Electrical resistivity	Ω cm	10^2 – 10^3	-	-	-	

Although the fabrication of 3C-SiC/Si epilayers appears to be quite attractive for leveraging the favourable characteristics of SiC at a low cost, the poor crystal quality of these epilayers, in contrast to what has been obtained on hexagonal bulk SiC wafers, has prevented their use in device fabrication. 3C-SiC remains on the market for a variety of applications due to a favourable trade-off between cost savings and an excellent opportunity for scalability versus worse quality compared to hexagonal polytypes. Due to the instability of 3C-SiC, it is transformed to 6H-SiC around 2100 °C. In addition, because of the instability of cubic-SiC, it is not easy to produce large amounts at a reasonable rate. Crystals of 2H-SiC are regarded as one of the rare crystalline silicon modifications. These crystals could measure 3.2 mm in the z-direction and 0.28 mm in the x-direction and are usually clear but may be colourless or chroma-coloured due to the reduction of methyl trichlorosilane in a hydrogen environment at 1300–1400 °C. The susceptor temperature profile and the presence of methyl trichlorosilane in hydrogen substantially impact the crystallisation of 2H-SiC. Using the first principle, the elastic constants, and electrical characteristics of 2H-SiC and 4H-SiC were determined. The calculation of the total energy of both polytypes revealed that their phases are comparable.

The finding demonstrated that 4H-SiC has a more rigid elasticity than 2H-SiC [15]. Even 2H-SiC substances are unstable at elevated temperatures, and it is not possible to synthesise large 2H-SiC crystals. Consequently, 4H-SiC and 6H-SiC polytypes are in vogue and have garnered significant attention [16]. Using molecular dynamic simulation based theoretical CASTEP code simulations, the effect of pressure on many SiC polytypes was investigated.

At room temperature, 10–200 GPa pressures were applied to 2H-SiC, 4H-SiC, and 6H-SiC. The induced pressure range did not modify the tetragonal lattice's shape, but compression changed its electrical and structural properties. As pressure rises, 4H-SiC and 6H-SiC bandwidth narrows [17]. 3C-SiC's bandwidth increased due to its high electron mobility, induced pressure sensitivity, and saturation velocity. Intermediate band solar cells often use Cubic-SiC as a buffer/window layer because of their bandgap. It has simple access to deep levels, a crucial requirement for a photovoltaic material [18].

Cubic-SiC has an inherent concentration of 10^{16} per cm^3 at 30 °C, allowing it to be utilised as a buffer layer in a solar cell instead of cadmium sulphide, together with molybdenum, tin oxide (window), and antimony triselenide (absorber) [19]. SiC polytypes have different electronic capabilities, leading to various electronic band frameworks and optoelectronic features. 4H-SiC is superior to other SiC polytypes for high-power and electronic device applications due to its high critical electric field strength and hole mobility. Therefore 4H-SiCs are utilised in power device applications. 6H-SiC possesses a robust covalent bond, high hardness, a low thermal expansion coefficient, and excellent thermal and chemical stabilities. This makes 6H-SiC excellent for precision nanomoulding dies and high-performance mirrors, where fast, easy manufacture with faultless surface integrity is crucial.

9R-SiC is a rhombohedral SiC. These have an identical microscopic and crystallographic nature to that of Cubic-SiC. 9R-SiC's band gap is greater than 2H-SiC due to its poor hexagonality. 9R-SiC has a higher conduction band, which makes it a strong choice for high-frequency and high-voltage applications [20]. 15R-SiC wafers are hard to procure despite their mobility for MOSFET devices. 15R-SiC growth requires a substrate. The C-face of 4H-SiC at 1750 °C and the Si-face of 6H-SiC at 1900 °C are used to grow 15R-SiC. The band structure, density of states, lattice parameter, and charge density of 15R-SiC were deduced using density functional theory based on the plane wave pseudopotential framework. The electrical structure and optical features were examined using estimated band structure and density of states. 15R-SiC is an indirect band gap semiconductor with a 2.16 eV charge density, which indicates that the Si-C bond is a hybrid bond semiconductor with an appropriate covalent bond but weak ionicity.

A natural superlattice, 21R-SiC has atomic-scale colour centres with controlled spin states via optical and microwave channels. In photoluminescence, spin-3/2 zero-phonon

lines vary in fine structure between the ground and excited states. Changes in photoluminescence intensity under magnetic resonance circumstances and the crossover of ground and excited spin levels open ventures in quantum computing, magnetometry, and thermometry [21]. Density functional theory was used to study the electrical structure and optical linear response function of 21R-SiC. The lattice parameter, density of states, complex dielectric function, energy band structure, and absorption coefficient establish a theoretical correlation between 21R-SiC's optical properties and electronic structure. The calculated energy band structure was utilised to evaluate 21R-SiC's dielectric function and extinction coefficient, giving a theoretical framework for designing photoelectric substances.

3. Synthesis of Silicon Carbide

3.1. Microwave Sintering

Moshtaghioun et al. [22] used microwave sintering to produce β -SiC nanoparticles from silicon dioxide and carbon. Before the reaction, the mixture of carbon and silicon dioxide particles was milled for 40 h to enhance the reaction activity and lower the heat input. The milled mixture was subjected to microwave sintering at 1200 °C for 5 min to generate β -SiC (ϕ —15–30 nm) with 98.5% purity, as shown in Figure 4.

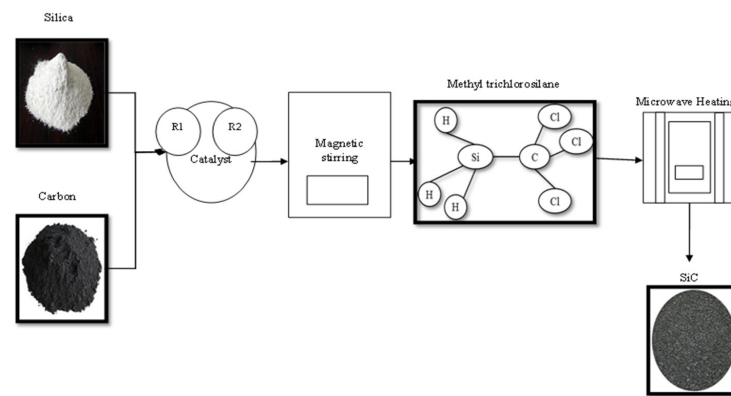


Figure 4. Microwave sintering of silicon carbide nanoparticles.

Zhan et al. [23] used microwave sintering to synthesise β -SiC at 1650 °C for 1 h with a purity of 75.7%. During the execution, the microwave oven was coupled with infrared thermal support to generate β -SiC. Furthermore, they found that a surge in the residence time and temperature favoured the production of β -SiC. SiC nano-whiskers were generated using microwave sintering of graphite and silica in a ratio of 1:3 at 1400 °C for 0.5 h. The mechanism used in this process was a vapour solid since no catalyst was deployed. α - and β -SiC were generated using a microwave heating approach with coal mineral particles as the carbon source and tetra-ethoxy-silane as the silicon source at 1100 °C for 10 min [24].

3.2. DC Arc Discharge Plasma

Pak et al. [25] used DC arc discharge plasma to transform silica and carbon into SiC. The procedure used a carbon-electrode along with an electric-arc reactor, as shown in Figure 5. The 100 Å DC arc between the graphite rod and crucible in ambient air was applied to a ball-milled combination of cubic silica and charcoal, generating 26.7% SiC. Adjusting the arc discharge current amplitude changes phase composition and SiC yield. The arc discharge's volt-ampere properties were examined with a dual-channel oscilloscope. The first channel tracked voltage, and the second channel tracked current.

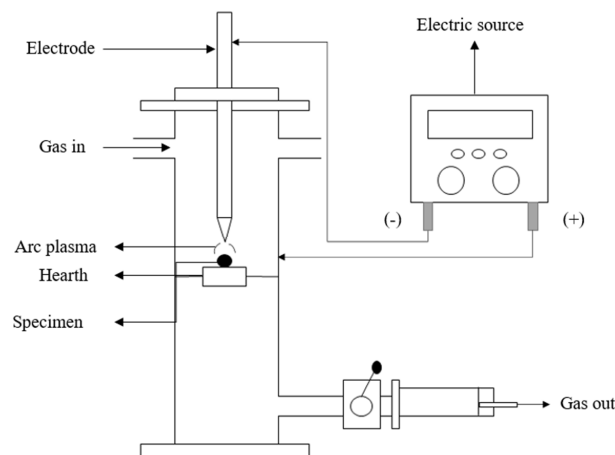


Figure 5. Schematic representation of arc discharge plasma.

Integrating voltage and current to draw a power curve determined dissipated energy. Infrared thermometers recorded the temperature every 2 s till 1850 °C. The current was held constant while the impregnation ratio (Si:C = 1:4, 1:2, 1:1, and 2:1), residence period (10–30 s), and arc discharge trials were varied (1–3). When this triple-fold arc approach is applied at 220 Å for 25–30 s, silicon and carbon are converted to SiC.

3.3. Detonation Technique

Langenderfer et al. [26] implemented an approach to synthesise nano-diamonds of SiC that involved a mild steel pressure tank as a detonator. The charge was formulated by blending equal quantities (120 g) of both TNT and RDX that had been previously melted in separate boilers at 100 °C. An amount of 10 g of poly-carbo-silane was added to the TNT and RDX mix. The charge was cast in a hollow cylindrical container, and the cast material was suspended in the vessel's middle. To begin the charge, the reaction vessel was cleansed with argon. After detonation, the vessel was shut for 0.17 h to allow the amorphous carbon to settle, as represented in Figure 6. The vessel was then opened, the amorphous carbon was collected, and the solid particles sank to the bottom. The supernatant was centrifuged at 4500 rpm to sediment the suspended particles for 0.75 h. The moisture was removed by placing them on a hot plate, followed by the addition of HCl to separate metal, metal oxides, and impurities. The acquired powder was then washed with distilled water and centrifuged till the pH of the wastewater approached 5. As a result, SiC was generated by using poly-carbo-silane to detonate explosives. The denoted soot contained amorphous carbon, nano-diamond, and silicon dioxide spheres.

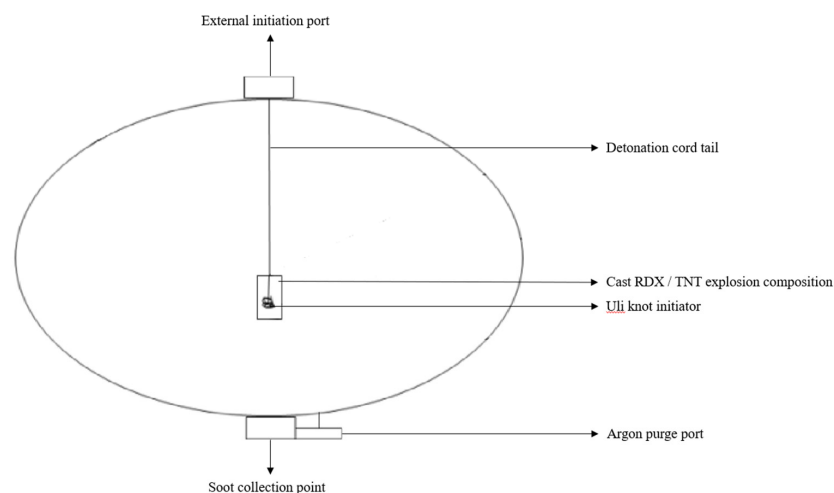


Figure 6. Detonation synthesis of silicon carbide.

3.4. Calcination Approach

Tan et al. [27] proposed a novel method for producing SiC by obtaining paper tissue (carbon-rich), spherical glass (silica-rich), and Fe (catalyst), then calcining it. The mixture was then made up of 0.15 g of $\text{Fe}(\text{NO}_3)_3 \cdot 9\text{H}_2\text{O}$ liquefied in 50 mL of water and 1 g of silica-rich material. The mixture was injected into the paper tissue (3.5 g) and dehumidified in a hot air oven at 100 °C for 10 h, as mentioned in Figure 7. The forerunners were then fed into a tubular reaction chamber and calcined for 2 h at 1600 °C in an argon atmosphere. To extract carbon, the chamber's output was sintered at 800 °C for 5 h. The iron and silica content were removed by injecting a blend of hydrogen chloride and hydrogen fluoride. Thus, SiC was synthesised using a calcination approach. This research opens new possibilities for recycling wastepaper and glass into low-cost microwave absorber nanomaterials.

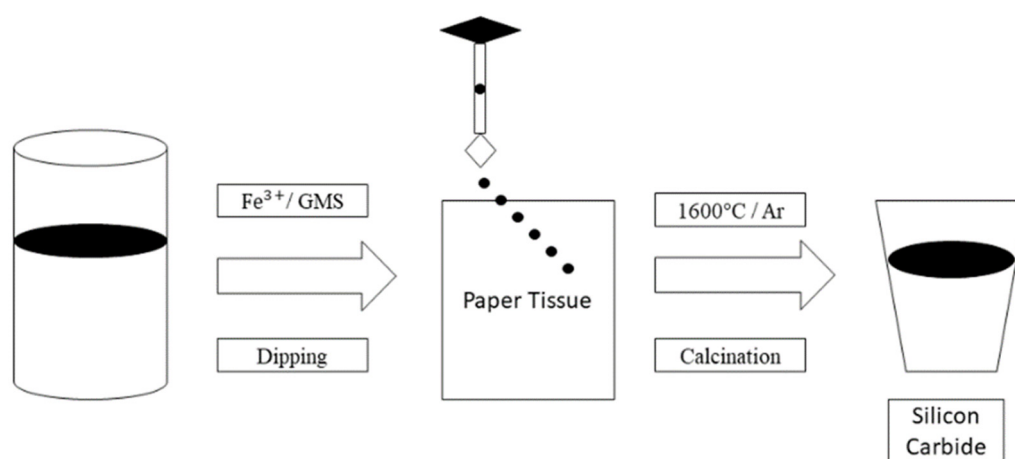


Figure 7. Calcination approach to generate silicon carbide.

3.5. Pyrolysis Technique

Rajarao et al. [28] synthesised porous β -SiC Nanoparticles (ϕ —20–80 nm) using waste macadamia shells as the carbon source and silica at 800 °C in an argon atmosphere. Sun et al. [29] presented a method for creating SiC using solid residue (carbon) and sandstone (silica) powder. The residue was procured from EtOH-SCC mining. The superfluous was cleansed with ethanol to remove the available liquid tar and then dehydrated at 60 °C for 12 h to separate the ethanol, followed by cooling the materials to atmospheric temperature and grinding them to a particle size of 250 μm . Later, the residue was strained with HCl and sintered at 75 °C for 48 h to separate the metallic impurities. After that, it was cooled, filtered, and washed with ion-free distilled water. The sandstone specimens, acquired from the Plumbago Creek silica sand sediment, were size reduced to 75 μm . Hydrochloric acid was sprinkled to remove the metallic particles from the sandstone powder. The cleansed residue and the sandstone grains were sintered at 1300–1600 °C for 1–3 h in an argon environment to produce SiC. The extra carbon in the SiC was removed by heating it at 850 °C for 6 h. It was demonstrated that a ball-milled sample of rice husk heated at 1500 °C for 2 h in an argon atmosphere yielded 69.2% SiC whiskers and SiC particulates [30]. The generation of porous β -SiC was carried out by utilising corn stover and sandstone as initiators in an aluminium crucible at 1700 °C for 4 h under an argon gas flow of 50 $\text{mL}\cdot\text{min}^{-1}$ [31]. By pyrolysing organo-silicas, SiC with a large specific surface area of 100 $\text{m}^2\cdot\text{g}^{-1}$ can be formed.

3.6. Molten Salt Synthesis Strategy

β -SiC nanowires (ϕ —10–50 nm) were produced by heating the silicon (partial reaction with $\text{NaF}:\text{NaCl} = 10:1$) and graphite in the ratio of 1:2 at 1400 °C for 3 h. SiC was generated on the surface of the graphite to prevent the oxidation of the inner graphite. The energy requirement for this process can be reduced from 1400 to 1150 °C if the raw material is coated with black carbon. The diameter of the SiC can be changed by varying the silica

and carbon black fractions. Molten silicon and carbon react at 1100–1300 °C in a mixture of 95% KCl and 5% sodium fluoride in an argon environment to synthesise SiC on the surfaces of the graphite flakes [32]. Silicon and graphite powders are fed into a corundum furnace at 1200 °C to synthesise necklace-shaped SiC/SiO_x heterojunctions that contain both SiC/SiO₂ (ø—0.3–1 µm) and Beans-SiO₂ (ø—2–5 µm). The generated products have the potential to be used in violet blue-emitting devices [33].

3.7. Sputtering Approach

The synthesis of SiC thin films with high adhesive strength by the amalgamation of metal vapour vacuum arc ion-source implantation and ion beam-assisted deposition was fulfilled by pre-treating the silicon with carbon at an ion hypnotic power of 5×10^6 ions·cm⁻². In another scenario, the targets were carbon (Mz grade) and silicon (5N purity), and they were subjected to sintering at 700 °C with a pressure of 1 Pa to synthesise SiC with excellent chemical and optical characteristics. A radio frequency magnetron co-sputtering approach was used for producing amorphous SiC films for use as a solar cell passivation layer. The target for this method is silica and carbon to deposit the film on p-type silicon (100) and glass substrates at room temperature. The emergence of crystalline and amorphous SiC films is proved using a single-composite target magnetron sputter deposition technique.

To attain controllable C content in the SiC films, the graphite coverage area was varied between 5 and 15%, with stoichiometry achieved at 12.85%. With no external heat during deposition, the films on Si substrates crystallised into 21H-SiC. SiC films deposited on quartz substrates under the same process parameters are amorphous. These films have an optically measured band gap of 3.4 eV, a refractive index of 1.96 at 1300 nm, and a high transparency of 85% in visible and near-infrared regions [34].

3.8. Solvothermal Synthesis

One-dimensional SiC was produced in an autoclave at 600 °C by a Mg-catalysed co-reduction of silicon-tetrachloride and 2-ethoxyethanol. Researchers tested the solvothermal preparation of 1D (nanorods, nanobelts, nanowires) and 2D SiC nanomaterials (nanosheets and hollow spheres). SiC composites can be made from extra carbon sources. SiC nanoparticles can be primed with waste plastics, creating a new path for plastic recycling. Using iodine and sulphur as additions lowered the processing temperature, highlighting the solvothermal method's uniqueness. The pyrolysis of polymethyl silane at 550 °C has been used to produce SiC nanoflakes and nanowires via a solvothermal technique. The nanostructures have high photoluminescence at 405–425 nm under 340 nm excitation wavelength [35].

3.9. Replica Technique

The porous carbon and silicone oil were sintered at 1600 °C for 1 h in an inert atmosphere to yield 40% of coated SiC. This approach was considered simple, and feedstocks were inexpensive, making the process viable for industrial applications. Organic foam impregnation produced SiC reticulated porous ceramics, with polyurethane sponges as templates and deionised water or alcohol as slurry solvents. The impregnation route comprises two stages; the first stage is where the raw materials are fed into a furnace at 700 °C, followed by sintering at 1800 °C in an argon environment.

The apparent density, sintering behaviour, and microstructures of the framework of SiC reticulated porous ceramics formed with aqueous slurry under different sintering aids and sintering processes, as well as the alcohol slurry, were compared. The test results demonstrated that the apparent density and microstructure of the samples produced with Y₂O₃ + AlN as a sintering aid were superior to those formed with Al₂O₃ as a sintering aid. The samples generated using alcohol slurry provided optimal properties for the aqueous slurry [36].

3.10. Siliconising Method

This is a method of synthesising textile-shaped β -SiC. The process involves siliconised silicon fabric with silicon monoxide vapour at 1400 °C with a pressure of 0.09 Pa to produce a combination of cubic (3C-SiC) and hexagonal SiC (6H-SiC). SiC fibres have a high mechanical tensile strength of 1470 MPa, a nanoscale hardness of 10 GPa, and an elastic modulus of 110 GPa [37].

3.11. Solid State Approach

3C-SiC and 6H-SiC were generated using a solid-state approach by utilising silica and activated carbon at 1300 °C for 6 h at 98 wt% [38]. Ugraskan et al. [39] proposed a solid-state method for producing high-quality SiC with a particle size of 850 nm. The solid-state method entails the reaction of three different materials: mixed waste glass (silica), magnesium, and graphite (carbon) with an impregnation ratio of 1:3:1, which were fed into the ball mill for size reduction. The milled mixture was heated at 600 °C for 14 h in an aluminium furnace in argon with a heating rate of 10 °C·min⁻¹, as represented in Figure 8. The resulting grey powder of SiC was washed with 5 M hydrochloric acid to remove the impurities. The acidity and basic constants of SiC were recorded as 0.086 and 0.077 for this specific study.

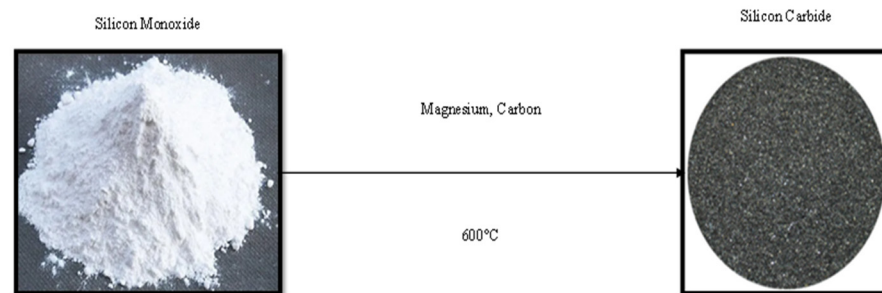


Figure 8. Solid-state synthesis of silicon carbide.

3.12. Carbothermal Reduction

The carbothermal reduction technique involves the usage of graphite flakes and microfine silica in equal proportions as feedstocks. They were fed into a reactor at 1300–1850 °C for 2 h in the presence of noble gas to generate SiC, as represented in Figure 9. The removal of surplus carbon can be accomplished by heating at 950 °C for 1 h in an oxidising environment. This is a promising solution since it eliminates the need for acid leaching prior to installation. In another scenario, the raw materials used for the process were silica xerogels and carbon, fed into a furnace at 1400 °C for 2 h to yield SiC nanowires (ϕ —50–400 nm).

Zhong et al. [40] utilised activated carbon and silicon dioxide particles to generate SiC nanoparticles (ϕ —20–30 nm) at 1500 °C. These SiC nanoparticles demonstrated agglomeration. Incorporating 3 wt% lanthanum as a catalyst during the reaction reduces the activation energy from 695 J·g⁻¹ to 295 J·g⁻¹, and the temperature required declined to 1360 °C from 1530 °C. To synthesise SiC, the carbothermal reduction requires a high temperature near the melting point of silicon dioxide. As a consequence, the silicon dioxide particles are prone to coalescence, resulting in a product with an unfavourable morphology. To mitigate the concern of agglomeration, a core-shell structure was proposed. This structure primarily encased silicon dioxide in carbon to maintain adequate contact between the reactants while allowing the particles to scatter without conglomeration.

In order to prevent fatal crashes in the chemical industry, fuel cell applications, and engine tests, it is essential to find hazardous and flammable gases rapidly and precisely in harsh environments. SiC is a promising candidate for gas-sensing devices used in harsh environments.

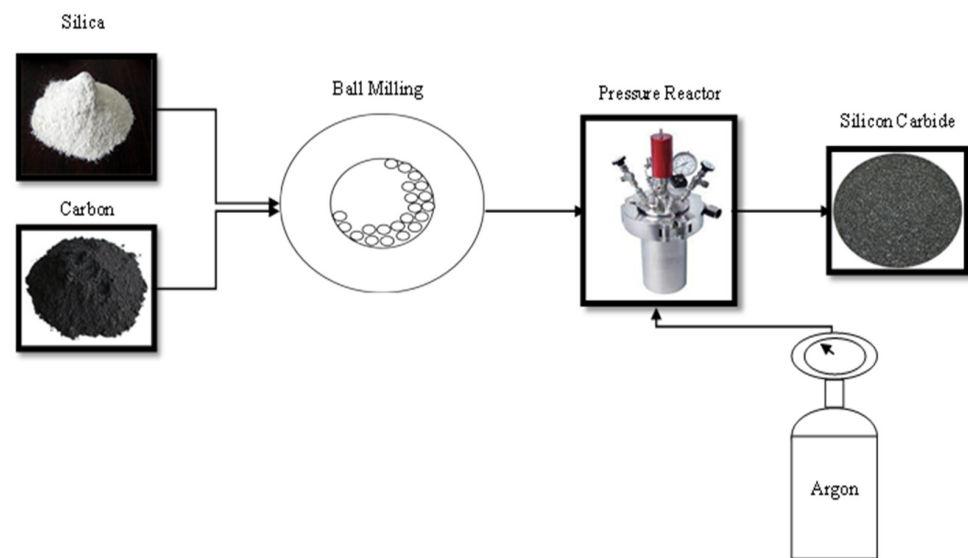


Figure 9. Carbothermal synthesis of silicon carbide nanoparticles.

Ceballos-Mendivil et al. [41] proposed a carbothermic reduction technique that could produce a nanostructure of β -SiC at 1500 °C for 2 h in an argon environment using SiO_2/C nanocomposite. This has resulted in the introduction of a low-carbon dioxide emission approach that has provided a significant amount of active carbon for composite development and is more thermally stable. A mixed sol of coal fly ash, water glass, and activated carbon (a carbon source) was employed in a furnace at 1500 °C for 4 h to create nano-whiskers of SiC. The efficiency of this approach was 75% [42].

To synthesise cubic and hexagonal SiC with a surface area of $863 \text{ m}^2 \cdot \text{g}^{-1}$, *Ecklonia Radiata* macroalgae were fed into an alumina crucible at 1550 °C for 15 min [43].

3.13. Chemical Vapour Deposition

Chemical vapour deposition (CVD) is widely used in material manufacturing because of its low deposition temperature, ease of operation, and low maintenance costs. CVD uses hexamethyl-disilyl amine as the precursor and nitrogen as the carrier gas to deposit SiC coatings on C/C composite substrates at 750–1500 °C for 2 h. The surge in temperature will create smoother SiC. Deposition temperature affects phase transition, coating shape, and structure. The cold-wall technique produces densely packed and crystallised SiC films. β -SiC nanowires require a catalyst with 100 nm thickness and a temperature of 600 °C [44].

A greyish film of β -SiC nanorods (ϕ —10–30 nm) could be formed on the silicon surface at 2200 °C for 2 h by making use of solid carbon and silicon in a warm filament CVD. The precursor dicarba-closo-dodecaborane reacts with the Si substrate to generate amorphous-SiC nano springs and helical nanowires in a plasma-enhanced CVD approach. CVD was used to create flower shaped SiC nanostructures. The silicon substrate and gallium nitride powder were fed into a tube furnace at 1000 °C, and the advent of methane gas triggered the expansion of the nanostructures. By using a gas phase reaction, the generation of β -SiC monocrystalline thin films (ϕ —0.4–1.7 μm) via CVD at 1400 °C at 1 atm was implemented.

In conclusion, this path generates SiC with relatively large surface areas from gaseous forerunners. Nevertheless, this strategy consumes a lot of energy, and scalability is impossible. As a result, there is an opportunity to pursue gas phase approaches that are quick, high-yielding, and have low energy consumption. Table 2 represents the synthesis techniques and their influential parameters of silicon carbide.

Table 2. Synthesis of silicon carbide along with their process parameters.

	Process Condition	Methodology	Form of SiC	Yield (%)	Diameter (nm)/ Particle Size (μm)	References
1	1200 °C; 0.1 h		Beta	98.5	15–30 nm	[22]
2	1650 °C; 1 h		Beta	75.7	-	[23]
3	220 Å; $3-8 \times 10^{-3}$ h	Microwave sintering	Powder	-	-	[24]
4	1600 °C; 2 h		SiC	-	-	[27]
5	800 °C		Beta	-	80 μm	[28]
6	1300–1600 °C; 1–3 h		SiC	-	-	[29]
7	1500 °C; 2 h		Nanowhiskers	69.2	-	[30]
8	1800 °C	Replica	Nanorods	-	-	[36]
9	1400 °C	Siliconising	Textile-Beta	-	-	[37]
10	1500 °C	Carbothermal redox	SiC	-	20–30 μm	[40]
11	1500 °C; 2 h		Beta	-	-	[41]
12	600 °C		Nanowires-Beta	-	100 μm	[44]
13	1400 °C		Nanopowders	-	20–40 μm	[45]
14	1400 °C; 0.5 h	Sol–Gel	Nanowires	-	-	[46]
15	1500 °C; 1 h		Strands-Beta	-	8.2–300 nm	[47]
16	1400 °C; 3 h		Beta	-	-	[48]
17	1650 °C; 1 h		SiC	-	10 nm	[49]
18	1500 °C; 5 h		Mesoporous	-	-	[50]
19	1500 °C; 1 h	Thermal evaporation	Nanoporous	-	50–200 nm	[51]
20	1700 °C; 1 h		Nanowires	-	20 nm, 2 μm	[52]
21	1100 °C; 2 h	Sputtering approach	Nanoclusters	-	165 μm	[53]
22	1800–1950 °C	Carbothermal reduction	Porous—40–55%	-	0.003–30 μm	[54]
23	1250–1350 °C		Nanostructured	-	-	[55]
24	750–1500 °C; 2 h	CVD	Coatings	-	-	[56]

3.14. Sol-Gel Technique

Najafi et al. [45] synthesised SiC nanopowder with a surface area of $171.4 \text{ m}^2 \cdot \text{g}^{-1}$ and particle size of 20–40 nm using liquefied precursors of tetraethyl orthosilicate (silicon-rich), Resol (carbon-rich), and hydrochloric acid as a catalyst. Ammonium polycarboxylate was used as a dispersant during gelation to limit product size and maintain solution durability. When the $\text{pH} < 4$, the solution was stable and formed β -SiC nanoparticles (ϕ —1–10 nm). On the contrary, when the PH surged from 4 to 7, the solution stability lowered, and the particle size increased. Sol–gel reactants are hydrolysed and gelled for homogeneous mixing. During the sintering of the gel to make SiC nanoparticles, gradient-oriented nucleation is possible, leading to the formation of SiC whiskers or nanowires.

3.15. Other Synthesis Techniques

3.15.1. Synthesis of Nanoparticles of SiC

Radiofrequency inductively heated plasma synthesises fine SiC nanopowder (ϕ —30–100 nm) from organic precursors (tetra-ethyl-orthosilicate, Hexa-methyl-disilane, and vinyl-trimethoxy-silane). To remove the impurities that existed in the SiC, they were subjected to thermal and hydrofluoric acid treatment [57]. A modified sol–gel method was used to synthesise ultrafine SiC nanoparticles at 1450 °C, and Si/C (1:1) was formed. The feedstock utilised was binary carbonaceous silicon xerogel and ferric nitrate as catalysts [58]. A femtosecond pulsed laser ablation technique was utilised for the synthesis of 4H-SiC (ϕ —2.84 nm) with a pulse width of 35 femtoseconds, a repetition rate of 1 kHz, a wavelength of 800 nm, and a single pulsed energy of 3.5 mJ focused by the lens at a residence time of 1.5 h. The value of the nonlinear absorption coefficient was found to be $3 \times 10^{-13} \text{ m} \cdot \text{W}^{-1}$ [59]. A controlled generation of pyramid-shaped SiC nanoparticles (ϕ —5–20 nm) was implemented by the carbonate contamination of the silicon surface

at a temperature range of 780–880 °C in the absence of oxygen. The density of the SiC nanoparticles can be altered by varying the amount of the carbonate species that are being deposited on the top layer of the silicon surface [60]. A molten salt electrosynthesis process generated SiC nanoparticles (ϕ —8–14 nm) from ultrafine silicon dioxide and carbon in molten calcium dichloride at 900 °C [61].

3.15.2. Synthesis of Nanowhiskers of SiC

SiC whiskers sprouted on the inner surface of the crucible after heating at 1600 °C for 3 h under 0.11 MPa under an argon environment and quick cooling. SiC whiskers generate when Si in FeSi and FeSi₂ melt films react with carbon diluted from the graphite furnace [62]. C-SiC composite nanowhiskers were generated via molten salt synthesis from Si powders, graphite as feedstock, and salt medium as NaF at 1300 °C for 3 h. SiC whiskers 10–50 nm long grew on the flake graphite surface, and the oxidation activation energy was 45.72 kJ·mol⁻¹ [63]. SiC nanowhiskers were fabricated at 1400 °C for 0.5 h at a heating rate of 20 °C·min⁻¹ by making use of graphite and silica with a ratio of 1:3 [46]. Microwave sintering by utilising graphite and silica in a ratio of 1:3 fed into a furnace synthesised SiC nanowhiskers at 1400 °C for 0.67 h [64]. Microwave heating of silica and graphite in the ratio of 1:3 in a hot plate at 1400 °C for 0.33–1 h obtained SiC nanowhiskers with minimal weight loss of 6% and band gap of 2.8 eV [65]. Nanowhiskers of SiC were formed by microwave heating of silica and graphite with a ratio of 1:3 at 1350–1450 °C for 40 min. The optimised temperature was 1400 °C, and the absorption bands of Si-C were present at 803.5/cm [66].

3.15.3. Synthesis of Nanowires of SiC

β -SiC nanowires (ϕ —10–25 nm) with uniform amorphous SiO₂ wrappers (ϕ —20–70 nm) and a length of 20 μ m have been produced by carbothermal reduction of the sol-gel derived silica containing carbon nanoparticles. The acquired β -SiC nanowires depend on the higher quantities of SiC nuclei and the nanometre-sized SiC nucleus sites on carbon nanoparticulates [67]. SiC nanowires can be synthesised by utilising silicon and phenolic resin as feedstock and sintering it at 1450 °C in the presence of argon with a constant flow rate of 50 mL·min⁻¹. The diameter and Young's modulus of the SiC nanowires ranged from 215 to 400 nm and 559.10 to 576.50 GPa, respectively [68].

The pyrolysis technique was used to generate huge quantities of pure 3C-SiC nanowires by using SiO₂/Si (silica-rich source) and graphene oxide (carbon-rich source) at 1350 °C for 3 h [69]. Nanowires of SiC with a diameter of 30–80 nm were fabricated by a direct reaction of graphene nanosheets with Si and SiO vapours at 1500 °C without a catalyst [70]. β -SiC nanowires were fabricated with a diameter of 80–100 nm using silica powder and ethanol as feedstock and ferrocene as a catalyst at 1550 °C for 2 h [71].

3.15.4. Synthesis of Nanofibres of SiC

Wang et al. [72] evaluated heat-resistant Tyranno SA/SiC composites synthesised by chemical vapour infiltration. At 2000 °C, composites retained 58% of their flexural strength. Zhao et al. [73] treated 3D polymer impregnation, and pyrolysis KD-I fibres reinforced SiC with a bending strength of 514.1 MPa at 1400 °C for 1 h in an inert environment. Lu et al. [74] generated 3D SiC_f/SiC composites with polycarbosilane and KD-I fibres as the reinforcement. The composite's ultimate tensile strength was 339.70 MPa at 1300 °C without oxidation. The electrospinning approach was implemented by making use of polycarbosilane as feedstock and toluene as a solvent to synthesise SiC fibres with an average diameter of 10.40 μ m [75]. Large quantities of 2H-SiC with diameters of 200–800 nm and small quantities of 3H-SiC with a length of 3–15 μ m were synthesised by sintering silicon nitride in the presence of argon at 1800 °C and 190 MPa [76]. A siliconising approach was used to fabricate SiC fibres at 1400 °C by using SiO gaseous vapour and carbon cloth as raw material. The obtained SiC fibre was like the morphology of the carbon texture [77].

3.15.5. Synthesis of SiC Using Polycarbosilane

The ceramic conversion of liquid polycarbosilane at 1300 °C under an argon environment obtained β -SiC with a crystallite size of 2 nm. Liquid polycarbosilane obtained as a by-product of polycarbosilane synthesis via a catalytic route was a viable SiC precursor for chemical liquid vapour deposition processes [78]. Selective solvent precipitation of high-molecular-weight polycarbosilane yields β -SiC micro powders. Polydimethylsiloxane was pyrolysed to form polycarbosilane (>3000 Da). Fine polycarbosilane powders (ϕ —10–100 μ m) were sintered at 1200–1450 °C in argon. Polycarbosilane-high molecular weight is thermally stable. β -SiC particles were inert up to 1000 °C and reactive above that temperature [79]. Polymeric and oligomeric carbosilanes with Si atoms linked by methylene groups were employed to make nano-sized tubules and bamboo-like SiC structures by chemical vapour deposition and liquid precursor infiltration as well as pyrolysis inside nanoporous alumina filter discs, followed by dissolving the alumina framework in aqueous hydrofluoric acid.

SiC nanotubes had 200–300 nm outer diameters, 20–40 nm wall thicknesses, and 60 μ m lengths. Chemical vapour deposition-derived SiC nanotubes annealed at 1600 °C in an argon environment provided nanocrystalline β -SiC or β -SiC/C composites in the shape of the source nanotubes, whilst liquid precursor-derived nanostructures converted to single crystal SiC nanofibers [80]. In an electrospinning approach, polycarbosilane fibres with a diameter of 1 μ m were calcined at 1200 °C for 2 h to transform into β -SiC fibres with a diameter of 0.8 μ m [81].

Polycarbosilane precursor was subjected to sintering at 1200 °C to generate 85% of β -SiC and trace quantities of α -cristobalite [82]. The chemical vapour deposition technique was employed for converting polycarbosilane films into polycrystalline β -SiC when heated at 200–1200 °C under a vacuum pressure of 10 torrs. The thickness of the polycarbosilane should always be less than 1 μ m to avoid extensive cracking, thereby minimising the cost of transformation [83].

3.15.6. Synthesis of SiC Using In Situ Reaction Synthesis

SiC–Boron nitride composites were synthesised via the in situ technique that utilised silicon nitride, boron carbide, and carbon as feedstocks. The in situ process was advantageous for obtaining better composites with fine grain size and homogeneous microstructures. The SiC (25 vol%) doped with boron nitride via the in situ approach had a peak strength of 588 MPa, comparable with the monolithic SiC (peak strength—620 MPa). These in situ SiC–BN composites might have superior thermal shock resistance and mechanical strain tolerance [84].

Tetraethoxysilane in N-methyl morpholine-N-oxide-dissolved cellulose. Such solutions have a lower viscosity than neat cellulose solutions. This makes composite fibres conceivable in cellulose solution. Introducing 10% tetra-ethyl-oxy-silane in a cellulose matrix does not modify fibre strength, but the modulus of elasticity rises from 20% to 30%. It enables the thermal treatment of composite precursors to generate C-SiC fibres [85]. A spark plasma sintering method was utilised by making use of titanium, silicon, and carbon as raw materials to fabricate SiC at a faster rate with a grain size of 100 nm. The produced SiC did not form by direct interaction of silica and carbon, but it actually formed during the intermediate phase of the process [86]. SiC particulates (ϕ —0.2–10 μ m) were synthesised by the in situ reaction of liquid–solid aluminium–silicon–carbon alloys at 750 °C. The particle size is positively correlated to the temperature of the approach [87].

4. Purification Approaches of Silicon Carbide

4.1. Thermal Treatment

Acid leaching and heat treatment extracted metallurgical-grade silicon from ingot sludge waste. Hydrofluoric acid and hydrochloric acid were used for leaching to eliminate the metal contaminants. The remaining SiC was sorted by melting point using 1600 °C in an inert environment, and the purity of silica was 99.70% [88]. The higher fatigue strength

of 218.52 MPa was observed for the composite specimen comprising 9 wt% of SiC_p and 4 wt% of fly ash at a sintering temperature of 670 °C, at a stirring speed and duration of 100 rpm and 15 min, respectively. The fatigue life cycle of the composites ranged from 9.29×10^5 cycles to 2.64×10^9 cycles under the conditions mentioned earlier [89]. SiC powder, along with excess carbon, was synthesised at 1550 °C from a Si sludge-to-C (1:1.4). To remove excess carbon from the obtained SiC, the product was heat-treated in the air at 750 °C for 5 h. The carbon was either removed as carbon monoxide or carbon dioxide when heated in the oxygen environment [90].

The induction heating process ingeniously combines the merits of different heating rates with superior purification phenomena and minimal material consumed. The induction heating process was subjected to 1300 °C for 5 h in a vacuum state. At the end of the initial heat preservation stage, high-purity argon was injected to maintain a constant pressure of 100–150 torr, and then the temperature was increased to 1650 °C for 5 h. Then, the temperature again surged to 2050 °C for 15 h. In the final stage, the temperature was slowly decreased to ambient temperature. Thus, a high-quality SiC source with a minimal weight loss of 6.7% and contaminants, such as Al, B, Fe, Mg, Na, and Ti, in the range of 1.10 ppm was observed [91].

4.2. Acid Leaching

The investigation involved the utilisation of sulphuric acid as the leaching agent for removing the iron and aluminium from quartz sand (silica-rich). The optimal leaching rates for iron and aluminium were 98% and 94%, respectively, after thermal treatment at 100 °C for 2 h. The impregnation ratio of solid to liquid was 1:4, and the grain size of quartz was between 0.125 mm to 0.250 mm [92]. The impact of introducing hydrogen peroxide as an oxidising agent on cleansing metallurgical grade silicon by leaching with hydrofluoric acid was examined as a function of leaching temperature, particle size, leaching duration, and leaching agent concentration.

Hydrogen peroxide in hydrofluoric acid lixiviant increased the removal ability for metallic contaminants without affecting hydrofluoric acid concentration. Leaching with 1 mol·L⁻¹ hydrofluoric acid and 2 mol·L⁻¹ hydrogen peroxide at 55 °C for 0.25 h improved metallurgical grade silicon purity from 99.74% to 99.96%, and subsequent leaching improved it to 99.99% [93].

4.3. Flotation

Mean and median particle sizes are 3.98 µm and 1.71 µm before flotation and 9.30 µm and 9.70 µm after flotation. Flotation can recover SiC from waste silicon slurry. The effective hydrofluoric concentrations of 0.80 mol·L⁻¹ for the first stage and 0.60 mol·L⁻¹ for the second stage lead to a SiC recovery efficiency of 76.60%. In a two-stage flotation process, the ideal oxidation-reduction potential is −400 mV for the initial stage and −300 mV for the secondary, allowing 84.30% SiC recovery efficiency. At an ideal hydrofluoric acid concentration, 52.80% of SiC was recovered [94].

5. Properties of Silicon Carbide

5.1. Biomimetic Properties of Silicon Carbide

SiC biomaterials are employed in biosensing and optoelectronics due to their physical and thermo-mechanical properties. The material SiC has a high modulus of elasticity (425 GPa), a high hardness (46 GPa), and a low coefficient of friction (0.16). Moreover, it is a ceramic material appropriate for high chemical conditions, whereas amorphous ceramics have a thermal stability limit of 245 °C. SiC is biocompatible due to its broad bandgap of 2.5–3.1 eV based on polytype (2H-SiC, 4H-SiC, 6H-SiC, 15R-SiC, and 21R-SiC) and its chemical inertness that resists corrosion under harsh temperatures. To increase the creep resistance and endurance of oxide-free SiC, boron and carbon are added. Boron- and carbon-doped SiC is a suitable material for biomedical implants [95] due to the exclusion of grain boundaries. Physicochemical features of natural resources generated from plants

with potential biological applications include mechanical properties, stiffness, stretchability, lightweight, and abrasion resistance.

The biomimetic synthesis approach entails a reaction of carbonaceous biopreform and infiltrating silicon melt at 1200 °C in the presence of oxygen to obtain biomorphic Si-SiC ceramic composites with flexural strength and Young's modulus of 264 MPa and 247 GPa. Si-SiC composites were converted into porous (49 vol.%) SiC ceramics by depleting the surplus silicon phase in channel apertures with carbon. SiC-based materials can be used for structural applications and in designing filters that can withstand extreme temperatures and photocatalysts [96]. The morphologies, grain size, pore orientation, and pore size of these substances make them an exciting component in the biomedical sector due to their physicochemical characteristics.

5.2. Surface Properties of SiC

Observations indicate that SiC nanoparticles have a greater specific surface area than bulk materials. These features of nanoparticles have a substantial impact on their chemical stability and homogeneity, affecting their uses.

Several scientists, for instance, analysed the surface properties of SiC nanoparticles. Nanocomposites' surface properties are essential for the creation of stable colloidal solutions and ceramic slurries. However, biosynthetic approaches such as the pulsed laser ablation method can manufacture SiC nanoparticles with enhanced hydrophilicity but mass-producing SiC nanoparticles is challenging. Changing the surface of SiC nanoparticles is one strategy for addressing the problems.

Organic and inorganic SiC nanoparticle modifications are the most common. Transplanting organic molecules onto the surface of SiC particles primarily constitutes the primary organic modification [97]. A layer of biotic material was placed on the exterior of modified SiC nanoparticles to prevent the nanoparticles from agglomeration and to enhance the adhesive strength of the SiC-resin interface.

In terms of inorganic modification, Saini et al. [98] modified SiC nanoparticles with concentrated nitric acid. C—O (1701/cm), -C—C- (1538/cm), and C—O (1185/cm) are present in the changed SiC, which may be the result of nitric acid oxidation. Surface treatment can alter the properties of SiC nanocomposites, allowing them to be utilised in current nanocomposites, innovative materials, and functional ceramics. Surface porosity and high surface area are the two most important characteristics of SiC ceramics for defining their surface properties. The characteristics of SiC nanocomposites can be modified using surface treatment, enabling them to be utilised in modern nanocomposites, novel materials, and functional ceramics. Surface porosity and high surface area are the key features of SiC ceramics for determining surface properties [99]. The surface properties of materials must be determined to explain wettability, cohesion, and adhesiveness. Furthermore, determining properties is critical for making the assessed materials suitable for industrial applications. Flow microcalorimetry, contact angle, and liquid adsorption can all be used to investigate surface attributes. Inverse gas chromatography at infinite dilution approaches is commonly employed by researchers. There is a need for a more detailed study to represent that SiC has exceptional surface properties and can be utilised for diverse applications.

5.3. Thermal Properties of SiC

Due to its high melting point (2700 °C) and chemical resistance, SiC is suited for high-temperature applications. Due to the size effect, nanoparticles have a huge surface area, resulting in a significant variation in thermal characteristics. Nano-thermodynamics has been developed to bridge the gap between macroscopic and nanoscale systems. Nano-thermodynamics of metal nanocrystals have been researched in depth. Huseynov et al. [100] examined the thermal breakdown of β -SiC nanoparticles using thermogravimetric analysis. The relationship between the mass of SiC nanoparticles and temperature at various heating rates was studied.

Due to their substantial specific surface area, SiC nanoparticles can absorb water and other compounds in the air. Initially, when the temperature increases, these adsorbed pollutants are removed, resulting in a decrease in sample mass. The sample's mass increased as the temperature exceeded 800 °C, owing to SiC oxidation. Then, the effect of neutron radiation on the thermal behaviour of β -SiC nanoparticles was studied [101].

Timofeeva et al. [102] investigated the impact of surfaces and particle size on SiC's thermal conductivity. The surface energy of nanoparticles does not affect their thermal conductivity, as demonstrated by the research. Given the same volume% and an increase in nanoparticle particle size from 6 nm to 90 nm, their thermal conductivity surged. It was found that particle size was positively correlated to thermal stability. Due to their better thermal stability at 800 °C and radiation resistance, SiC nanoparticles can be used in the aerospace and nuclear energy domains.

5.4. Electrical Properties of SiC

SiC is a semiconductor with exceptional electrical characteristics that make it ideal for semiconductor devices with high frequency. The side effect has been shown to have an impact on the material's electrical properties, and some SiC nanoparticles possess distinctive electronic characteristics, including dielectric constant and conductivity. The impact of frequency and temperature on the electrical characteristics of β -SiC nanoparticulates was studied by See et al. [103].

The dielectric constant of SiC steadily declined as the frequency increased. Furthermore, there was no correlation between the surge in temperature and the dielectric constant of SiC that could be explained by the bandgap theory's simple electron hopping. It has been noticed that element doping substantially influences the dielectric constants of SiC nanoparticles. To date, scientists have created Co, Fe, Cu, Ni, and N-doped SiC nanoparticles to enhance their dielectric constant. The variation in atomic valence creates corresponding voids, and the dielectric constant becomes escalated whenever these compounds reach the SiC lattice and substitute Si atoms. For instance, Fe atoms are trivalent, indicating they have three electrons that bind with supplementary compounds.

A p-type material with Fe-Si imperfections was formed if Si atoms were substituted by iron atoms in SiC, which improved the dielectric constant. Huseynov et al. [104] also revealed that neutron irradiation could innovate doping in SiC nanoparticulates, which improved the dielectric constant. On the other hand, Huseynov et al. [105] tested the influence of neutron irradiation, frequency, and temperature on SiC nanoparticle conductivity. Whenever the frequency was 0.95 kHz, the conductivity did not vary, but when the frequency was 2 kHz, it increased correspondingly. When the frequency was reduced to 1 kHz, the conductance of SiC nanoparticles inflated from $2 \times 10^{-6} \text{ S}\cdot\text{m}^{-1}$ (100 K) to $8 \times 10^{-5} \text{ S}\cdot\text{m}^{-1}$ (400 K), implying that towering temperature and frequency can cause SiC nanoparticles to develop more carriers. They also discovered that neutron radiation caused a nuclear phase shift in silicon atoms, resulting in the production of ^{31}P , which improved the concentration of n-type donors as well as improved conductivity. To conclude, neutron irradiation and doping can enhance the electrical properties of SiC nanoparticles, expanding their horizons in diverse fields.

6. Applications of SiC

6.1. Wastewater Treatment-Based Applications of SiC

Wastewater management is a vital sector with environmental challenges that require immediate attention. Vegetable oil waste from numerous sources, especially the food industry, pollutes the air, water, and soil. Fraga et al. [106] synthesised first-generation and second-generation SiC membranes with unique top layers to separate oily wastes. These commercially made membranes remove suspended particles, grease, and oil from industrial effluent. For molecular separation, ceramic membranes are used in petrochemical, beverage and food processing, water purification, bioreactors, and chemical manufacturing.

SiC's high chemical and thermal stability has attracted several industries. Current energy demand and environmental deterioration have pushed scientists to investigate hydrogen as an environmentally benign option. Commercial hydrogen generation necessitates using a large number of fossil fuels, which emit greenhouse gases that contribute to global warming.

For the development of innovative solutions, photocatalytic water-splitting techniques have emerged as a viable option for hydrogen production. Diverse compounds were utilised for artificial photosynthesis in the presence of a photocatalyst, and a vast amount of research was conducted. Most metal oxides respond more effectively to ultraviolet rays than to visible light due to their larger band gap. Thus, there is an urgent need for visible-light-driven photocatalysts capable of creating hydrogen through artificial photosynthesis. The semiconductor's bandgap must be between 1.23 eV and 3.0 eV for this to be possible. SiC is the optimal material because of its bandgap (2.3–3.3 eV) and good physical and chemical properties. The three different morphologies of SiC (whiskers, vermiform, and particles) are robust, and they possess acceptable photocatalytic efficiency under ultraviolet irradiation for hydrogen generation via artificial photosynthesis in the absence of a sacrificial agent.

Initially, Au nanoparticles decorated with SiC nanowire hybrids were formed via deposition–precipitation at 350 °C for 2 h. Disodium sulphate was used as a sacrificial reagent in water under simulated sunshine from a 300 W xenon lamp. Over the composition-optimised Au/SiC composite (with 0.5 wt% Au), the photoactivity for hydrogen evolution ($1495.8 \mu\text{mol}\cdot\text{h}^{-1}\text{g}^{-1}$) was increased significantly along with apparent quantum efficiency of 2.12%. Au (0.5 wt%)/SiC composite exhibited superior photocatalytic and structural stability in cycle tests. Photoluminescence, time-resolved photoluminescence, and photoelectrochemical analysis revealed enhanced charge separation and recombination acted as a way to enhance the photocatalytic and photoelectrochemical performances of SiC [107,108].

6.2. Composite-Based Applications

Wang et al. [109] described the development of a silicon nanoporous pillar array (Si-NPA), a silicon micro-nanometre structural composite model comprised of arrayed nanoporous silicon pillars. Various temperature and gas sensors with excellent sensitivity, short response times, and minimal hysteresis have been manufactured using Si-NPA or its nanocomposite materials as sensing substrates. These results indicate that Si-NPA could be utilised as a sensing element and as a prototype for producing sensing materials.

A large quantity of SiC nanowires (ϕ —15 nm) was generated utilising a catalyst-assisted CVD technique on Si-NPA. At ambient temperature, the humidity sensor capabilities of SiC nanowires/Si-NPA were studied by evaporating interdigital coplanar silver electrodes onto the surface of the specimen. At 100 Hz, a capacitance gain of 958% was only achieved when the relative humidity rose from 10% to 94%. Response and recovery times were 110 s and 90 s, respectively, and the most significant relative humidity hysteresis was 4.5% at 75% relative humidity. It has been demonstrated experimentally that SiC nanowires/Si-NPA sensors exhibit exceptional measurement reproducibility and long-term stability.

Ceramic fillers can provide electrical insulation due to their high thermal conductivity and moderate electrical conductivity. SiC ceramics can serve as fillers due to their outstanding thermal conductivity of $90 \text{ W}\cdot\text{m}^{-1}\text{K}^{-1}$, exceptional thermal endurance, low thermal expansion coefficient, superior mechanical properties, and exceptional chemical durability. The high dielectric constant (40 MHz at 1 MHz) limits its use in fully interconnected electronic packaging systems for applications involving fast signal transfer. Yang et al. [110] developed a 20% loaded epoxy resin nanocomposite containing SiC nanoparticles with a conductivity of just $0.8 \text{ W}\cdot\text{m}^{-1}\text{K}^{-1}$.

6.3. SiC Used for Energy Applications

Designers of spintronic devices have shown an interest in diluted magnetic semiconductors. Typically, they are produced by doping with magnetic metallic elements. SiC may

be mature enough for higher power and more advanced electrical circuits, making it a crucial diluted magnetic semiconductor.

Seong et al. [111] fabricated V-shaped SiC nanowires that were only slightly magnetic and lacked a hysteresis loop at 5K. Tian et al. [112] created single-crystalline Mn-doped 3C-SiC nanowires from powders of Si, SiO₄, Mn, and graphite. The magnetisation was analysed as a function of the magnetic field curves at 5K and 300K. In the case of Mn-doped SiC nanowires, the hysteresis loops at 5K and 300K demonstrate conclusively that the sample possesses substantial ferromagnetic ordering.

Mn-doped 3C-SiC nanowires can exhibit ambient temperature ferromagnetism. The results of the superconductor interferometric device indicate that nanowires exhibited room-temperature ferromagnetism behaviour. The ambient temperature ferromagnetism property of nanowires facilitates their use in spintronic devices.

6.4. Medical Applications of SiC

SiC bioceramics are appropriate for use in biomedical implants due to their bio-inertness, as well as their user-friendliness, mouldability, physical stability, non-reactivity, and biocompatibility. This SiC biomaterial may also be used to coat total hip replacements, ortho implants, and artificial heart valves. Recent efforts have been focused on the three-dimensional printing of bio-inert ceramic materials based on SiC.

Si micro-matching provides SiC with superior chemical and mechanical properties, enabling its usage in hip implants and prosthetic bone replacement. These cast ceramic materials are used as body components and to aid in life-saving therapies [113].

Cancer is one of the deadliest diseases, with many different forms of cancer progression and only a few medications available to treat them, although not totally. Nanoparticles made of 3C-SiC are one of the most intriguing strategies for combating cell proliferation. SiC nanoparticles could be utilised as active antiproliferative agents for cancer diagnostics. Nevertheless, cytotoxicity is arguably the most prevalent concern connected with SiC-based nanoparticles, and it is unknown if SiC-based nanomaterials can handle crucial problems and Si.

Current advances in three-dimensional tissue engineering have caught the attention of scientists studying its applications in the bio-derived medical field. It is difficult for 3D biomedical engineering to create complicated artificial organs using three-dimensional tissue constructs that can absorb nutrition and dispose of waste [114]. Most of them are constructed without using sacrificial spacers for various reasons, including cost, inconvenient methods, and time. When exposed to ultraviolet light coupled with a photo-initiator, this produces chemicals that are harmful to cells.

6.5. Applications of Non-Stoichiometric SiC

The silicon-rich Si_xC_{1-x} films were fabricated in a low-energy plasma-amplified CVD reactor with a silane-rich atmosphere. By adjusting the radio frequency strength of the plasma, it appears possible to tune the silicon molar ratio, resulting in a range of materials with various Si/C ratios. The absorbance of the Si_xC_{1-x} films was between 400 nm and 600 nm, whereas the band gap was observed between 1.49 eV and 2.05 eV. The material's performance was also evaluated for solar components, with lower series resistance, better efficiency, and shunt resistance upon reduction of the film's diameter. The higher absorption of visible electromagnetic radiation by silica-rich SiC thin films indicates the material's potential for use in electronics. Designing SiC ring-wave-guide resonators for use as data format followers or as an inverter [115].

Majid et al. [116] investigated the surfaces (1010) and (1120) of the material using a self-consistent charge-dependent tight-binding technique derived from second-order density functional theory. Surfaces under standard temperature and pressure are found to be semiconducting, while specific non-stoichiometric reconstructions have metallic properties. All the silicon atoms in the first layer were replaced with carbon atoms, resulting in a carbon-terminating material and a violation of stoichiometry.

As the Si-Si bond is longer than the Si-C bond, the Si-terminating surface proved stable across a broad temperature range. In contrast, the carbon-terminating surface was only stable in conditions with a higher carbon fraction. The Si terminating surface was found to be metallic, with a silicon equivalent state positioned 0.5 eV above the valence band maximum. In contrast, the carbon-terminating surface exhibited a carbon-associated state at 2.9 eV above the Fermi level; the valence band maximum was deemed semiconducting. The applications of silicon carbide, as well as their influencing characteristics, are shown in Table 3.

Table 3. Cont.

	Applications	Process Condition	Particle Size (nm)/Porosity (%)	Thickness (μm)/Diameter (mm)	Parameters	References
17	Field effect transistors (Channel transistor)	-	4.1 nm	-	1457, 1132, 980 $\mu\text{A}\cdot\mu^{-1}\text{m}^{-1}$ (P-type) 229, 35, 21 $\mu\text{A}\cdot\mu^{-1}\text{m}^{-1}$ (N-type)	[135]
18	Field effect transistors (Epitaxial bilayer)	25–200 °C	-	-	40 GHz (Max. oscillation frequency)	[136]
19	Metal semiconductor field effect transistor with bulgy channel	-	-	-	63.76% (Breakdown voltage) 72.85% (Max. output power density) 4.42% (Cutoff frequency)	[137]
20	Metal semiconductor field effect transistor with p-type doing	-	-	-	30% (Bulgy channel), 78% (Breakdown voltage) 137% (Max. output power density) 18% (Characteristic frequency)	[138]
21	Cleaning method	-	12,000 nm	150 mm	150 mm (4H-SiC)	[139]
22	Electrochemical (Mechanical polishing)	-	-	-	14.54 $\mu\text{m}\cdot\text{h}^{-1}$ (Material removal rate) 4.5X (>Electrochemical) 290X (>Mechanical)	[140]
23	Electrochemical capacitance	-	-	-	3.1 Ω (Low charge transfer resistance) 3.2 $\text{mF}\cdot\text{cm}^{-2}$ (Areal capacitance value) 100 $\text{mV}\cdot\text{s}^{-1}$ (Cycle voltammetry cycle) 50 $\text{mV}\cdot\text{s}^{-1}$ (Scan rate)	[141]
24	Catalyst	20 min	-	-	62 $\mu\text{m}\cdot\text{h}^{-1}$ (Material removal rate) 163.33 to 25.45 nm (Surface roughness)	[142]
25	Electrochemical performance	-	-	-	5 wt% catalyst, 200 $\text{F}\cdot\text{g}^{-1}$ at 0.5–3 $\text{A}\cdot\text{g}^{-1}$ (Specific capacitance)	[143]
26	Lithium-ion batteries (Anode material)	-	400–600 nm	-	>99% (Coulombic efficiency) 1000 $\text{mA}\cdot\text{h}\cdot\text{g}^{-1}$ (Specific capacity) 0.5 $\text{A}\cdot\text{g}^{-1}$ (Charge discharge rate) 98.06% (Coulombic efficiency)	[144]
27	Lithium-ion batteries with electrochemical stability	-	-	-	748.2 $\text{mA}\cdot\text{hg}^{-1}$ (Initial discharge capacity) 0.1 $\text{A}\cdot\text{g}^{-1}$ (Charge discharge rate) 816.3 $\text{mA}\cdot\text{hg}^{-1}$ (Reverse capacity) at 100 cycle 1.0 $\text{A}\cdot\text{g}^{-1}$ (Charge discharge rate)	[145]
28	Electrochemical corrosion	-	8170–22,420 nm	-	0.44 $\text{gm}\cdot\text{cm}^{-2}\text{hr}^{-1}$ (Degradation rate)	[146]
29	Nuclear fusion reactor (Composite)	1323 MPa	-	-	(Infiltrated Tungsten Copper) 2 wt%–SiC	[147]
		1380 °C, 3 h, 9:1 (Si:SiO ₂)	600–800 nm	-	0.373 (Highest particle–particle contiguity) 34% (Conversion rate of carbon to SiC) >94% (SiO gas)	[148]
30	Light water reactor	300 °C, 15 MPa	-	-	5.1 MeV (Irradiated Chemical Vapour Deposition)	[149]
31	Fusion ceramic welds	1450 °C	-	-	160–200 Å, 36.9 \pm 1.3 Vol% SiC	[150]
		1700 °C, 600 MPa	-	-	3–4 $\text{MPa}\cdot\text{m}^{0.5}$ (Before welding) 2–2.5 $\text{MPa}\cdot\text{m}^{0.5}$ (After welding), 40–60% (Strength)	[151]

Table 3. Cont.

Applications	Process Condition	Particle Size (nm)/Porosity (%)	Thickness (μm)/Diameter (mm)	Parameters	References
32	3D printing	600 °C	-	Room Temp, 4 GHz, -57 db, 3 GHz, -15 db 2.7–3.9 GHz (Max. Electromagnetic wave absorption bandwidth) -16–64 db (Min. electromagnetic wave reflection coefficient)	[152]
33	Catalyst (Hydrogen production)	-	-	2248.5 $\mu\text{L}\cdot\text{h}^{-1}\text{g}^{-1}$ (Photoreaction rate)	[153]
34	Automobile brakes	120–153 MPa	6%	2.1 (Individual platinum loading) 2.3 $\text{g}\cdot\text{cm}^{-3}$ (Density), 0.33 (SFC)	[154]
35	High-speed trains (Brake pads)	-	-	33 stops at 14 m/s, 93.1% (Coefficient of friction)	[155]
		-	-	8 stops at 55 m/s, 98.9% (Coefficient of friction) 0.443 at 37 m/s, 0.486 at 55 m/s, 0.460 at 69 m/s,	[156]
		1.25 MPa	-	0.469 (HMFC), 0.895 (SC), 0.147–0.338 $\text{cm}^3\cdot\text{MJ}^{-1}$ 200–350 $\text{Km}\cdot\text{h}^{-1}$	[157]

7. Conclusions and Future outlooks

This review emphasises the synthesis, characteristics, and utilisation of SiC nanomaterials. The shape of as-received raw materials, sintering method, processing temperature, particle size, and process parameters influences the synthesised product of SiC. Homogeneity in the obtained SiC can be challenging to attain. The synthesis of SiC had temperatures ranging from 750 °C to 1800 °C, and a residence time of 1–6 h with or without catalyst was discussed. Electrical, biomimetic, biocompatibility, and thermal properties of SiC were described to use in divergent applications.

Further research is essential to determine the relationship between cubic, hexagonal, and rhombohedral SiC structure and performance. This allows the selection of SiC nanoparticles with the required performance for nanodevices. SiC nanoparticles' cytotoxicity must be examined further for medicinal and biological applications. Researchers must study SiC's performance at extreme temperatures.

There is a need for research in the generation of α -SiC because substantial investigation has been undertaken in the β -SiC. SiC's tribological and mechanical characteristics must be analysed for different applications. Researchers should focus on solid-state systems that can produce SiC at lower temperatures. SiC nanoparticles are employed in composites, catalysts, bioadhesives, etc., due to their exceptional characteristics. Most of these applications remain under investigation, but they have promising applications. This requires extensive research, constructive interaction, and coordination between scholars.

Author Contributions: The designing, editing, and reviewing of the manuscript was performed by M.G. The manuscript was drafted and edited by A.V.T. All authors have read and agreed to the published version of the manuscript.

Funding: This research received no external funding.

Data Availability Statement: Not applicable.

Acknowledgments: We would like to express our sincere thanks to the Vellore Institute of Technology for offering us all the resources that were necessary.

Conflicts of Interest: The authors declare no conflict of interest.

References

1. Ram, C.; Kumar, A.; Rani, P. Municipal solid waste management: A review of waste to energy (WtE) approaches. *BioResources* **2021**, *16*, 4275–4320. [[CrossRef](#)]
2. Hossain, R.; Sahajwalla, V. Molecular recycling: A key approach to tailor the waste recycling for high-value nano silicon carbide. *J. Clean. Prod.* **2021**, *316*, 128344. [[CrossRef](#)]
3. Basov, D.N.; Averitt, R.D.; Hsieh, D. Towards properties on demand in quantum materials. *Nat. Mater* **2017**, *16*, 1077–1088. [[CrossRef](#)] [[PubMed](#)]
4. Acheson, E.G. Carborundum: Its history, manufacture and uses. *J. Franklin Inst.* **1893**, *136*, 194–203. [[CrossRef](#)]
5. Wang, D.; Li, Z.; Zhang, H.; Sun, J.; Tang, Y.; Huang, L. Plasmonic Au activates anchored Pt-Si bond in Au-Pt-SiC promoting photocatalytic hydrogen production. *J. Alloys Compd.* **2022**, *915*, 165450. [[CrossRef](#)]
6. Deshpande, A.; Chen, Y.; Narayanasamy, B.; Yuan, Z.; Chen, C.; Luo, F. Design of a high-efficiency, high specific-power three-level t-type power electronics building block for aircraft electric-propulsion drives. *IEEE J. Emerg. Sel.* **2020**, *8*, 407–416. [[CrossRef](#)]
7. Francis, A.M.; Holmes, J.; Chiolino, N.; Barlow, M.; Abbasi, A.; Mantooth, H.A. High-Temperature Operation of Silicon Carbide CMOS Circuits for Venus Surface Application. *Addit. Conf.* **2016**, *2016*, 000242–000248. [[CrossRef](#)]
8. Choi, W.-Y.; Yang, M.-K. High-efficiency design and control of zeta inverter for single-phase grid-connected applications. *Energies* **2019**, *12*, 974. [[CrossRef](#)]
9. La Via, F.; Severino, A.; Anzalone, R.; Bongiorno, C.; Litrico, G.; Mauceri, M.; Schoeler, M.; Schuh, P.; Wellmann, P. From thin film to bulk 3C-SiC growth: Understanding the mechanism of defects reduction. *Mater. Sci. Semicond. Process.* **2018**, *78*, 57–68. [[CrossRef](#)]
10. Nishino, S.; Powell, J.A.; Will, H.A. Production of large-area single-crystal wafers of cubic SiC for semiconductor devices. *Appl. Phys. Lett.* **1983**, *42*, 460–462. [[CrossRef](#)]
11. Pak, A.; Ivashutenko, A.; Zakharova, A.; Vassilyeva, Y. Cubic SiC nanowire synthesis by DC arc discharge under ambient air conditions. *Surf. Coat. Technol.* **2020**, *387*, 125554. [[CrossRef](#)]
12. Langenderfer, M.; Bohannan, E.; Watts, J.; Fahrenholtz, W.; Johnson, C.E. Relating detonation parameters to the detonation synthesis of silicon carbide. *J. Appl. Phys.* **2022**, *131*, 175902. [[CrossRef](#)]

13. Wang, Q.; Yokoji, M.; Nagasawa, H.; Yu, L.; Kanezashi, M.; Tsuru, T. Microstructure evolution and enhanced permeation of SiC membranes derived from allylhydridopolycarbosilane. *J. Membr. Sci.* **2020**, *612*, 118392. [[CrossRef](#)]
14. Nishioka, K.; Komori, J.; Maeda, K.; Ota, Y.; Kaneko, H.; Sato, K. Formation of silicon carbide using volcanic ash as starting material and concentrated sunlight as energy resource. *Int. J. Photoenergy* **2015**, *2015*, 1–4. [[CrossRef](#)]
15. Majid, A.; Rani, N.; Malik, M.F.; Ahmad, N.; Najam-al-Hassan; Hussain, F.; Shakoor, A. A review on transition metal doped silicon carbide. *Ceram. Int.* **2019**, *45*, 8069–8080. [[CrossRef](#)]
16. Kimoto, T. Bulk and epitaxial growth of silicon carbide. *Prog. Cryst. Growth Charact. Mater.* **2016**, *62*, 329–351. [[CrossRef](#)]
17. Pizzagalli, L. Accurate values of 3C, 2H, 4H, and 6H SiC elastic constants using DFT calculations and heuristic errors corrections. *Philos. Mag. Lett.* **2021**, *101*, 242–252. [[CrossRef](#)]
18. Sobayel, M.K.; Chowdhury, M.S.; Hossain, T.; Alkhamash, H.I.; Islam, S.; Shahiduzzaman, M.; Akhtaruzzaman, M.; Techato, K.; Rashid, M.J. Efficiency enhancement of CIGS solar cell by cubic silicon carbide as prospective buffer layer. *Sol. Energy* **2021**, *224*, 271–278. [[CrossRef](#)]
19. Metzger, W.K.; Grover, S.; Lu, D.; Colegrove, E.; Moseley, J.; Perkins, C.L.; Li, X.; Mallick, R.; Zhang, W.; Malik, R.; et al. Exceeding 20% efficiency with in situ group V doping in polycrystalline CdTe solar cells. *Nat. Energy* **2019**, *4*, 837–845. [[CrossRef](#)]
20. Yaghoubi, A.; Singh, R.; Melinon, P. Predicting the primitive form of rhombohedral silicon carbide (9R-SiC): A pathway toward polytypic heterojunctions. *Cryst. Growth Des.* **2018**, *18*, 7059–7064. [[CrossRef](#)]
21. Anisimov, A.N.; Babunts, R.A.; Breev, I.D.; Soltamov, V.A.; Mokhov, E.N.; Baranov, P.G. High-temperature spin manipulation on color centers in rhombic silicon carbide polytype 21R-SiC. *JETP Lett.* **2020**, *112*, 774–779. [[CrossRef](#)]
22. Moshtaghioun, B.M.; Poyato, R.; Cumbreira, F.L.; de Bernardi-Martin, S.; Monshi, A.; Abbasi, M.H.; Karimzadeh, F.; Dominguez-Rodriguez, A. Rapid carbothermic synthesis of silicon carbide nano powders by using microwave heating. *J. Eur. Ceram. Soc.* **2012**, *32*, 1787–1794. [[CrossRef](#)]
23. Zhan, H.; Zhang, N.; Wu, D.; Wu, Z.; Bi, S.; Ma, B.; Liu, W. Controlled synthesis of β -SiC with a novel microwave sintering method. *Mater. Lett.* **2019**, *255*, 126586. [[CrossRef](#)]
24. Zhang, F.; Chen, Y.; Wei, S.; Si, Y.; Wang, H.; Zhang, R.; Wang, G.; Song, L.; Fan, B. Microwave heating and mechanism for seed-induced synthesis of SiC. *Mater. Today Commun.* **2022**, *31*, 103846. [[CrossRef](#)]
25. Pak, A.Y.; Larionov, K.; Korchagina, A.; Yakich, T.Y.; Nalivaiko, A.Y.; Gromov, A. Silicon carbide obtaining with DC arc-discharge plasma: Synthesis, product characterization and purification. *Mater. Chem. Phys.* **2021**, *271*, 124938. [[CrossRef](#)]
26. Langenderfer, M.J.; Fahrenholtz, W.G.; Chertopalov, S.; Zhou, Y.; Mochalin, V.N.; Johnson, C.E. Detonation synthesis of silicon carbide nanoparticles. *Ceram. Int.* **2020**, *46*, 6951–6954. [[CrossRef](#)]
27. Tan, R.; Zhou, J.; Yao, Z.; Wei, B.; Li, Z. A low-cost lightweight microwave absorber: Silicon carbide synthesized from tissue. *Ceram. Int.* **2021**, *47*, 2077–2085. [[CrossRef](#)]
28. Rajarao, R.; Sahajwalla, V. A cleaner, sustainable approach for synthesising high purity silicon carbide and silicon nitride nanopowders using macadamia shell waste. *J. Clean. Prod.* **2016**, *133*, 1277–1282. [[CrossRef](#)]
29. Sun, K.; Wang, T.; Chen, Z.; Lu, W.; He, X.; Gong, W.; Tang, M.; Liu, F.; Huang, Z.; Tang, J.; et al. Clean and low-cost synthesis of high purity beta-silicon carbide with carbon fiber production residual and a sandstone. *J. Clean. Prod.* **2019**, *238*. [[CrossRef](#)]
30. Alweendo, S.T.; Johnson, O.T.; Shongwe, M.B.; Kavishe, F.P.L.; Borode, J.O. Synthesis, optimization and characterization of silicon carbide (SiC) from Rice Husk. *Procedia Manuf.* **2019**, *35*, 962–967. [[CrossRef](#)]
31. Wang, T.; Gong, W.; He, X.; Kou, Z.; Tan, G.; Zhou, S.; Yu, H.; Fan, M.; Kung, H.H. Synthesis of highly nanoporous β -silicon carbide from corn stover and sandstone. *ACS Sustain. Chem. Eng.* **2020**, *8*, 14896–14904. [[CrossRef](#)]
32. Masoudifar, S.; Bavand-Vandchali, M.; Golestani-Fard, F.; Nemati, A. Molten salt synthesis of a SiC coating on graphite flakes for application in refractory castables. *Ceram. Int.* **2016**, *42*, 11951–11957. [[CrossRef](#)]
33. Li, W.; Jia, Q.; Liu, X.; Zhang, J. Large scale synthesis and photoluminescence properties of necklace-like SiC/SiO_x heterojunctions via a molten salt mediated vapor reaction technique. *Ceram. Int.* **2017**, *43*, 2950–2955. [[CrossRef](#)]
34. Akshara, P.C.; Rajaram, G.; Krishna, M.G. Single composite target magnetron sputter deposition of crystalline and amorphous SiC thin films. *Mater. Res. Express* **2018**, *5*, 036410. [[CrossRef](#)]
35. Li, H.X.; Li, G.Y.; Hu, T.J.; Li, X.D.; Yang, Y.Q. Preparation of amorphous silicon carbide nanostructures via solvothermal method. *Appl. Mech. Mater.* **2014**, *597*, 49–52. [[CrossRef](#)]
36. Zhang, X.Z.; Wang, R.J.; Liu, G.W.; Shao, H.C.; Zhang, K.; Shi, Z.Q.; Qiao, G.J. Preparation of silicon carbide reticulated porous ceramics by organic foam impregnation. *Mater. Sci. Forum* **2015**, *814*, 574–578. [[CrossRef](#)]
37. Frolova, M.G.; Titov, D.D.; Lysenkov, A.S.; Kravchuk, K.S.; Istomina, E.I.; Istomin, P.V.; Kim, K.A.; Kargin, Y.F. Properties of silicon carbide fibers obtained by silicification of carbon fabric with SiO vapours. *Ceram. Int.* **2020**, *46*, 18101–18105. [[CrossRef](#)]
38. Mas'Udah, K.W.; Diantoro, M.; Fuad, A. Synthesis and structural analysis of silicon carbide from silica rice husk and activated carbon using solid-state reaction. *J. Physics: Conf. Ser.* **2018**, *1093*, 012033. [[CrossRef](#)]
39. Ugraskan, V.; Isik, B.; Yazici, O.; Cakar, F. Surface characterization and synthesis of boron carbide and silicon carbide. *Solid State Sci.* **2021**, *118*, 106636. [[CrossRef](#)]
40. Zhong, Y.; Shaw, L.L.; Manjarres, M.; Zawrah, M.F. Synthesis of silicon carbide nanopowder using silica fume. *J. Am. Ceram. Soc.* **2010**, *93*, 3159–3167. [[CrossRef](#)]

41. Ceballos-Mendivil, L.G.; Cabanillas-López, R.E.; Tánori-Córdova, J.C.; Murrieta-Yescas, R.; Pérez-Rábago, C.A.; Villafán-Vidales, H.I.; Arancibia-Bulnes, C.A.; Estrada, C.A. Synthesis of silicon carbide using concentrated solar energy. *Sol. Energy* **2015**, *116*, 238–246. [[CrossRef](#)]
42. Luo, Y.; Zheng, S.; Ma, S.; Liu, C.; Ding, J.; Wang, X. Novel two-step process for synthesising β -SiC whiskers from coal fly ash and water glass. *Ceram. Int.* **2018**, *44*, 10585–10595. [[CrossRef](#)]
43. Echeverria, C.A.; Pahlevani, F.; Lim, S.; Sahajwalla, V. Synthesis and characterization of biomorphic 1D-SiC nanoceramics from novel macroalga precursor material. *J. Clean. Prod.* **2021**, *312*, 127808. [[CrossRef](#)]
44. Leong, T.J.; Khalid, K.A.A.; Mohamed, K. Low temperature synthesis of silicon carbide nanowires on cathode for thermionic energy converter. *Mater. Today Proc.* **2019**, *7*, 704–709. [[CrossRef](#)]
45. Najafi, A.; Golestani-Fard, F.; Rezaie, H.R.; Saeb, S.P. Sol-Gel synthesis and characterization of SiC–B₄C nano powder. *Ceram. Int.* **2021**, *47*, 6376–6387. [[CrossRef](#)]
46. Lee, C.C.; Kahar, S.M.; Voon, C.H. Microwave synthesis of silicon carbide nanowhiskers: Effect of molar ratio. *Mater. Today Proc.* **2021**, *37*, 119–121. [[CrossRef](#)]
47. Ebadzadeh, T.; Marzban-Rad, E. Microwave hybrid synthesis of silicon carbide nanopowders. *Mater. Charact.* **2009**, *60*, 69–72. [[CrossRef](#)]
48. Ding, J.; Deng, C.; Yuan, W.; Zhu, H.; Zhang, X. Novel synthesis and characterization of silicon carbide nanowires on graphite flakes. *Ceram. Int.* **2014**, *40*, 4001–4007. [[CrossRef](#)]
49. Czosnek, C.; Bućko, M.M.; Janik, J.F.; Olejniczak, Z.; Bystrzejewski, M.; Łabędź, O.; Huczko, A. Preparation of silicon carbide SiC-based nanopowders by the aerosol-assisted synthesis and the DC thermal plasma synthesis methods. *Mater. Res. Bull.* **2015**, *63*, 164–172. [[CrossRef](#)]
50. Kong, Y.; Zhong, Y.; Shen, X.; Gu, L.; Cui, S.; Yang, M. Synthesis of monolithic mesoporous silicon carbide from resorcinol–formaldehyde/silica composites. *Mater. Lett.* **2013**, *99*, 108–110. [[CrossRef](#)]
51. Wei, J. Synthesis of nanoporous silicon carbide ceramics by thermal evaporation process. *Appl. Surf. Sci.* **2010**, *256*, 6626–6629. [[CrossRef](#)]
52. Niu, J.; Wang, J. An approach to the synthesis of silicon carbide nanowires by simple thermal evaporation of ferrocene onto silicon wafers. *Eur. J. Inorg. Chem.* **2007**, *25*, 4006–4010. [[CrossRef](#)]
53. Nussupov, K.K.; Beisenkhanov, N.B.; Seitov, B.Z.; Bakranova, D.I.; Keyinbay, S. The formation of SiC films by magnetron sputtering. *Phys. Sci. Technol.* **2018**, *5*, 23–28. [[CrossRef](#)]
54. Eom, J.-H.; Kim, Y.-W.; Song, I.-H.; Kim, H.-D. Microstructure and properties of porous silicon carbide ceramics fabricated by carbothermal reduction and subsequent sintering process. *Mater. Sci. Eng. A* **2007**, *464*, 129–134. [[CrossRef](#)]
55. Larpiattaworn, S.; Ngernchuklin, P.; Khongwong, W.; Pankurdee, N.; Wada, S. The influence of reaction parameters on the free Si and C contents in the synthesis of nano-sized SiC. *Ceram. Int.* **2006**, *32*, 899–904. [[CrossRef](#)]
56. Wu, S.; Kousaka, H.; Kar, S.; Li, D.; Su, J. Friction and wear performance of bearing ball sliding against diamond-like carbon coatings. *Mater. Res. Express* **2017**, *4*, 015602. [[CrossRef](#)]
57. Ko, S.-M.; Koo, S.-M.; Cho, W.-S.; Hwnag, K.-T.; Kim, J.-H. Synthesis of SiC nano-powder from organic precursors using RF inductively coupled thermal plasma. *Ceram. Int.* **2012**, *38*, 1959–1963. [[CrossRef](#)]
58. Omid, Z.; Ghasemi, A.; Bakhshi, S.R. Synthesis and characterization of SiC ultrafine particles by means of sol-gel and carbothermal reduction methods. *Ceram. Int.* **2015**, *41*, 5779–5784. [[CrossRef](#)]
59. Guo, X.; Song, H.; Li, Y.; Wang, P.; Liu, S. Fabrication of 4H-SiC nanoparticles using femtosecond pulsed laser ablation in deionized water. *Opt. Mater.* **2022**, *132*, 112817. [[CrossRef](#)]
60. Borowik, Ł.; Chevalier, N.; Mariolle, D.; Martinez, E.; Bertin, F.; Chabli, A.; Barbé, J.-C. Controlled synthesis of SiC nanoparticles from surface silicon contamination. *Thin Solid Films* **2012**, *527*, 133–136. [[CrossRef](#)]
61. Pang, Z.-Y.; Li, X.; Zhang, X.-Q.; Li, J.-J.; Wang, S.-J.; Xiong, X.-L.; Li, G.-S.; Xu, Q.; Zhou, Z.-F.; Zou, X.-L.; et al. Molten salt electrosynthesis of silicon carbide nanoparticles and their photoluminescence property. *Trans. Nonferrous Met. Soc. China* **2022**, *32*, 3790–3800. [[CrossRef](#)]
62. Yang, G.; Wu, R.; Chen, J.; Song, F.; Pan, Y. Growth of silicon carbide whiskers in FeSi₃ flux. *Mater. Chem. Phys.* **2007**, *106*, 236–239. [[CrossRef](#)]
63. Liu, Z.; Deng, C.; Yu, C.; Wang, X.; Ding, J.; Zhu, H. Preparation of in situ grown silicon carbide whiskers onto graphite for application in Al₂O₃-C refractories. *Ceram. Int.* **2018**, *44*, 13944–13950. [[CrossRef](#)]
64. Kahar, S.M.; Voon, C.H.; Lee, C.C.; Hashim, U.; Md Arshad, M.K.; Lim, B.Y.; Gopinath, S.B.; Rahman, W. Synthesis of SiC nanowhiskers from graphite and silica by microwave heating. *Mater. Sci.-Pol.* **2016**, *34*, 770–779. [[CrossRef](#)]
65. Kahar, S.M.; Voon, C.H.; Lee, C.C.; Gopinath, S.C.B.; Md Arshad, M.K.; Lim, B.Y.; Foo, K.L.; Hashim, U. Synthesis of silicon carbide nanowhiskers by microwave heating: Effect of heating duration. *Mater. Res. Express* **2017**, *4*, 015005. [[CrossRef](#)]
66. Voon, C.H. Synthesis of silicon carbide nanowhiskers by microwave heating: Effect of heating temperature. *Inf. MIDEM* **2017**, *47*, 101–112.
67. Meng, G.W.; Zhang, L.D.; Qin, Y.; Mo, C.M.; Phillipp, F. Synthesis of β -SiC nanowires with SiO₂ wrappers. *Nanostructured Mater.* **1999**, *12*, 1003–1006. [[CrossRef](#)]
68. Hu, P.; Dong, S.; Zhang, X.; Gui, K.; Chen, G.; Hu, Z. Synthesis and characterization of ultralong SiC nanowires with unique optical properties, excellent thermal stability and flexible nanomechanical properties. *Sci. Rep.* **2017**, *7*, 3011. [[CrossRef](#)]

69. Chen, S.; Li, W.; Qu, B.; Liu, X.; Wang, R.; Zhuo, D.; Wu, L. Synthesis of high-purity SiC nanowires via catalyst-free pyrolysis of SiO₂/Si and sponge-like graphene oxide. *ACS Omega* **2020**, *5*, 25319–25325. [[CrossRef](#)]
70. Hu, Z.; Chen, Z.; Huang, J.; Yan, M.; Zhang, M.; Zhang, L.; Li, X.; Feng, Z. Graphene-based SiC nanowires with nanosheets: Synthesis, growth mechanism and photoluminescence properties. *Crystrngcomm* **2020**, *22*, 4074–4078. [[CrossRef](#)]
71. Kao, K.; Jiang, M.; Ding, L.; Lin, W.; Chen, J. Catalytic synthesis of SiC nanowires in an open system. *J. Am. Ceram. Soc.* **2019**, *102*, 3070–3075. [[CrossRef](#)]
72. Wang, P.; Liu, F.; Wang, H.; Li, H.; Gou, Y. A review of third generation SiC fibers and SiCf/SiC composites. *J. Mater. Sci. Technol.* **2019**, *35*, 2743–2750. [[CrossRef](#)]
73. Zhao, S.; Zhou, X.; Yu, J.; Mummery, P. Effect of heat treatment on microstructure and mechanical properties of PIP-SiC/SiC composites. *Mater. Sci. Eng. A* **2013**, *559*, 808–811. [[CrossRef](#)]
74. Luo, Z.; Cao, H.; Ren, H.; Zhou, X. Tension-tension fatigue behavior of a PIP SiC/SiC composite at elevated temperature in air. *Ceram. Int.* **2016**, *42*, 3250–3260. [[CrossRef](#)]
75. Masripah; Zulys, A.; Setiawan, J. Synthesis of silicon carbide fiber as semiconductor substrate for Betavoltaic cell. *J. Physics: Conf. Ser.* **2018**, *1025*, 012129. [[CrossRef](#)]
76. Li, F.; Cui, W.; Zhang, J.; Du, S.; Chen, Z.; Zhang, S.; Chen, K.; Liu, G. Synthesis, characterization and growth mechanism of SiC fibers. *Mater. Chem. Phys.* **2022**, *291*, 126703. [[CrossRef](#)]
77. Istomina, E.I.; Istomin, P.V.; Nadutkin, A.V.; Kargin, Y.F.; Lysenkov, A.S. Preparation of a SiC Fiber textile material. *Inorg. Mater.* **2018**, *54*, 787–793. [[CrossRef](#)]
78. Nair, S.G.; Subramania Siva, M.; Thomas, D.; Sreejith, K.J.; Prabhakaran, P.V.; Devasia, R. Liquid polycarbosilane as a potential chemical liquid vapour deposition precursor for SiC. *Ceram. Int.* **2019**, *45*, 17442–17446. [[CrossRef](#)]
79. Krishnan, G.S.; Ramcharan, T.; Rao, R.R.; Naveen, S. Polymer-derived silicon carbide micro powders through selective solvent precipitation of high molecular weight polycarbosilane. *Ceram. Int.* **2021**, *47*, 17502–17509. [[CrossRef](#)]
80. Cheng, Q.-M.; Interrante, L.V.; Lienhard, M.; Shen, Q.; Wu, Z. Methylene-bridged carbosilanes and polycarbosilanes as precursors to silicon carbide—from ceramic composites to SiC nanomaterials. *J. Eur. Ceram. Soc.* **2005**, *25*, 233–241. [[CrossRef](#)]
81. Hu, S.; Yuan, J.; Wu, L.; Dai, H.; Ai, Y.; Deng, Y. Preparation and characterization of SiC fibers from PCS by electrospinning, curing and calcination process**. *Chemistryselect* **2021**, *6*, 11630–11637. [[CrossRef](#)]
82. Lodhe, M.; Babu, N.; Selvam, A.; Balasubramanian, M. Synthesis and characterization of high ceramic yield polycarbosilane precursor for SiC. *J. Adv. Ceram.* **2015**, *4*, 307–311. [[CrossRef](#)]
83. Colombo, P.; Paulson, T.E.; Pantano, C.G. Synthesis of silicon carbide thin films with polycarbosilane (PCS). *J. Am. Ceram. Soc.* **2005**, *80*, 2333–2340. [[CrossRef](#)]
84. Zhang, G.-J.; Ohji, T. In situ reaction synthesis of silicon carbide-boron nitride composites. *J. Am. Ceram. Soc.* **2004**, *84*, 1475–1479. [[CrossRef](#)]
85. Makarov, I.S.; Golova, L.K.; Mironova, M.V.; Vinogradov, M.I.; Bermeshev, M.V.; Berkovich, A.K.; Kulichikhin, V.G. Structural and morphological features of carbon—silicon-carbide fibers based on cellulose and triethoxyvinylsilane. *Fibre Chem.* **2018**, *50*, 79–84. [[CrossRef](#)]
86. Zhang, J.; Wang, L.; Shi, L.; Jiang, W.; Chen, L. Rapid fabrication of Ti₃SiC₂-SiC nanocomposite using the spark plasma sintering-reactive synthesis (SPS-RS) method. *Scr. Mater.* **2007**, *56*, 241–244. [[CrossRef](#)]
87. Du, X.; Gao, T.; Li, D.; Wu, Y.; Liu, X. A novel approach to synthesize SiC particles by in situ reaction in Al-Si-C alloys. *J. Alloy. Compd.* **2014**, *588*, 374–377. [[CrossRef](#)]
88. Kim, J.-Y.; Kim, U.-S.; Hwang, K.-T.; Cho, W.-S.; Kim, K.-J. Recovery of metallurgical silicon from slurry waste. *J. Korean Ceram. Soc.* **2011**, *48*, 189–194. [[CrossRef](#)]
89. Santhosh, N.; Kempaiah, U.N.; Sajjan, G.; Gowda, A.C. Fatigue Behaviour of silicon carbide and fly ash dispersion strengthened high performance hybrid al 5083 metal matrix composites. *J. Miner. Mater. Charact. Eng.* **2017**, *05*, 274–287. [[CrossRef](#)]
90. Hossain, S.T.; Johra, F.T.; Jung, W.-G. Fabrication of silicon carbide from recycled silicon wafer cutting sludge and its purification. *Appl. Sci.* **2018**, *8*, 1841. [[CrossRef](#)]
91. Fan, G.; Li, T.; Zhao, L.; Zhang, S. Study on purification technology of silicon carbide crystal growth powder. *Materials* **2022**, *15*, 8190. [[CrossRef](#)] [[PubMed](#)]
92. Boussaa, S.A.; Kheloufi, A.; Zaourar, N.B.; Bouachma, S. Iron and aluminium removal from algerian silica sand by acid leaching. *Acta Phys. Pol. A* **2017**, *132*, 1082–1086. [[CrossRef](#)]
93. Lai, H.; Huang, L.; Xiong, H.; Gan, C.; Xing, P.; Li, J.; Luo, X. Hydrometallurgical purification of metallurgical grade silicon with hydrogen peroxide in hydrofluoric acid. *Ind. Eng. Chem. Res.* **2016**, *56*, 311–318. [[CrossRef](#)]
94. Li, H.-C.; Chen, W.-S. Recovery of silicon carbide from waste silicon slurry by using flotation. *Energy Procedia* **2017**, *136*, 53–59. [[CrossRef](#)]
95. Xu, M.; Girish, Y.R.; Rakesh, K.P.; Wu, P.; Manukumar, H.M.; Byrappa, S.M.; Udayabhanu; Byrappa, K. Recent advances and challenges in silicon carbide (SiC) ceramic nanoarchitectures and their applications. *Mater. Today Commun.* **2021**, *28*, 102533. [[CrossRef](#)]
96. Chakrabarti, O.P.; Maiti, H.S.; Majumdar, R. Biomimetic synthesis of cellular SiC based ceramics from plant precursor. *Bull. Mater. Sci.* **2004**, *27*, 467–470. [[CrossRef](#)]

97. Saini, I.; Sharma, A.; Dhiman, R.; Chandak, N.; Aggarwal, S.; Sharma, P.K. Functionalized SiC nanocrystals for tuning of optical, thermal, mechanical and electrical properties of polyvinyl alcohol. *Thin Solid Film.* **2017**, *628*, 176–183. [[CrossRef](#)]
98. Saini, I.; Sharma, A.; Dhiman, R.; Ram, S.; Sharma, P.K. Structural and thermal characterization of polyvinylalcohol grafted SiC nanocrystals. *Mater. Res. Express* **2017**, *4*, 075015. [[CrossRef](#)]
99. Alvares, M.D.; Kakroudi, M.G.; Salahimehr, B.; Alaghmandfard, R.; Asl, M.S.; Mohammadi, M. Microstructure, mechanical properties, and oxidation behavior of hot-pressed ZrB₂-SiC-B₄C composites. *Ceram. Int.* **2020**, *47*, 9627–9634. [[CrossRef](#)]
100. Huseynov, E.M.; Naghiyev, T.G. Study of thermal parameters of nanocrystalline silicon carbide (3C-SiC) using DSC spectroscopy. *Appl. Phys. A* **2021**, *127*, 1–4. [[CrossRef](#)]
101. Huseynov, E.M.; Naghiyev, T.G.; Aliyeva, U.S. Thermal parameters investigation of neutron-irradiated nanocrystalline silicon carbide (3C-SiC) using DTA, TGA and DTG methods. *Phys. B Condens. Matter.* **2020**, *577*, 411788. [[CrossRef](#)]
102. Timofeeva, E.V.; Smith, D.S.; Yu, W.; France, D.M.; Singh, D.; Routbort, J.L. Particle size and interfacial effects on thermo-physical and heat transfer characteristics of water-based α -SiC nanofluids. *Nanotechnology* **2010**, *21*, 215703. [[CrossRef](#)]
103. See, A.; Hassan, J.; Hashim, M.; Wahab, Z.A.; Halim, D.N.F.A.; Abdullah, M.S.; Azis, R.S. Dielectric behavior of β -SiC nanopowders in air between 30 and 400 °C. *J. Mater. Sci. Mater. Electron.* **2016**, *27*, 6623–6629. [[CrossRef](#)]
104. Pourchez, J.; Forest, V.; Boumahdi, N.; Boudard, D.; Tomatis, M.; Fubini, B.; Herlin-Boime, N.; Leconte, Y.; Guillhot, B.; Cottier, M.; et al. In vitro cellular responses to silicon carbide nanoparticles: Impact of physico-chemical features on pro-inflammatory and pro-oxidative effects. *J. Nanoparticle Res.* **2012**, *14*, 1–12. [[CrossRef](#)]
105. Huseynov, E.M. Neutron irradiation effects on the temperature dependencies of electrical conductivity of silicon carbide (3C-SiC) nanoparticles. *Silicon* **2017**, *10*, 995–1001. [[CrossRef](#)]
106. Fraga, M.C.; Sanches, S.; Pereira, V.J.; Crespo, J.G.; Yuan, L.; Marcher, J.; de Yuso MV, M.; Rodríguez-Castellón, E.; Benavente, J. Morphological, chemical surface and filtration characterization of a new silicon carbide membrane. *J. Eur. Ceram. Soc.* **2017**, *37*, 899–905. [[CrossRef](#)]
107. Dang, H.; Li, B.; Li, C.; Zang, Y.; Xu, P.; Zhao, X.; Fan, H.; Qiu, Y. One-dimensional Au/SiC heterojunction nanocomposites with enhanced photocatalytic and photoelectrochemical performances: Kinetics and mechanism insights. *Electrochim. Acta* **2018**, *267*, 24–33. [[CrossRef](#)]
108. Zhang, Y.; Zhang, Y.; Li, X.; Dai, J.; Song, F.; Cao, X.; Lyu, X.; Crittenden, J.C. Enhanced photocatalytic activity of SiC-based ternary graphene materials: A DFT study and the photocatalytic mechanism. *ACS Omega* **2019**, *4*, 20142–20151. [[CrossRef](#)]
109. Wang, H.Y.; Wang, Y.Q.; Hu, Q.F.; Li, X.J. Capacitive humidity sensing properties of SiC nanowires grown on silicon nanoporous pillar array. *Sens. Actuators B Chem.* **2012**, *166–167*, 451–456. [[CrossRef](#)]
110. Yang, K.; Gu, M. Enhanced thermal conductivity of epoxy nanocomposites filled with hybrid filler system of triethylenetetramine-functionalized multi-walled carbon nanotube/silane-modified nano-sized silicon carbide. *Compos. Part A Appl. Sci. Manuf.* **2010**, *41*, 215–221. [[CrossRef](#)]
111. Seong, H.-K.; Park, T.-E.; Lee, S.-C.; Lee, K.-R.; Park, J.-K.; Choi, H.-J. Magnetic properties of vanadium-doped silicon carbide nanowires. *Met. Mater. Int.* **2009**, *15*, 107–111. [[CrossRef](#)]
112. Tian, Y.; Zheng, H.W.; Liu, X.Y.; Li, S.J.; Zhang, Y.J.; Hu, J.F.; Lv, Z.C.; Liu, Y.F.; Gu, Y.Z.; Zhang, W.F. Microstructure and magnetic properties of Mn-doped 3C-SiC nanowires. *Mater. Lett.* **2012**, *76*, 219–221. [[CrossRef](#)]
113. Li, T.; Li, X.-L.; Hu, S.-X.; Wu, J. Enhanced osteoporotic effect of silicon carbide nanoparticles combine with nano-hydroxyapatite coated anodized titanium implant on healthy bone regeneration in femoral fracture. *J. Photochem. Photobiol. B Biol.* **2019**, *197*, 111515. [[CrossRef](#)]
114. Attalla, R.; Ling, C.; Selvaganapathy, P. Fabrication and characterization of gels with integrated channels using 3D printing with microfluidic nozzle for tissue engineering applications. *Biomed. Microdevices* **2016**, *18*, 1–12. [[CrossRef](#)] [[PubMed](#)]
115. Su, S.-P.; Wu, C.-L.; Cheng, C.-H.; Huang, B.-J.; Wang, H.-Y.; Tsai, C.-T.; Lin, Y.-H.; Chi, Y.-C.; Shih, M.-H.; Lee, C.-K.; et al. Nonstoichiometric SiC Bus/Ring Waveguide Based All-Optical Data Format Follower and Inverter. *ACS Photon.* **2016**, *3*, 806–818. [[CrossRef](#)]
116. Majid, A. A perspective on non-stoichiometry in silicon carbide. *Ceram. Int.* **2018**, *44*, 1277–1283. [[CrossRef](#)]
117. Trevisan, M.; Vicente, J.; Ghidossi, R.; Vincent, A.; Moulin, P. Membrane characterisation from the support to the skin layer: Application to silicon carbide (SiC) membranes. *J. Eur. Ceram. Soc.* **2022**, *42*, 3759–3769. [[CrossRef](#)]
118. Trevisan, M.; Ghidossi, R.; Moulin, P. Silicon carbide (SiC) membranes in oenology. *Sep. Purif. Technol.* **2022**, *284*, 120276. [[CrossRef](#)]
119. Wang, F.; Hao, S.; Dong, B.; Ke, N.; Khan, N.Z.; Hao, L.; Yin, L.; Xu, X.; Agathopoulos, S. Porous-foam mullite-bonded SiC-ceramic membranes for high-efficiency high-temperature particulate matter capture. *J. Alloy. Compd.* **2022**, *893*, 162231. [[CrossRef](#)]
120. Huang, L.; Qin, H.; Hu, T.; Xie, J.; Guo, W.; Gao, P.; Xiao, H. Fabrication of high permeability SiC ceramic membrane with gradient pore structure by one-step freeze-casting process. *Ceram. Int.* **2021**, *47*, 17597–17605. [[CrossRef](#)]
121. Zhang, B.; Tong, Z.; Yu, H.; Xu, H.; Chen, Z.; Li, X.; Ji, H. Flexible and high-temperature resistant ZrO₂/SiC-based nanofiber membranes for high temperature thermal insulation. *J. Alloy. Compd.* **2021**, *872*, 159618. [[CrossRef](#)]
122. Jiang, Q.; Zhou, J.; Miao, Y.; Yang, S.; Zhou, M.; Zhong, Z.; Xing, W. Lower-temperature preparation of SiC ceramic membrane using zeolite residue as sintering aid for oil-in-water separation. *J. Membr. Sci.* **2020**, *610*, 118238. [[CrossRef](#)]
123. Wang, L.; Zhao, Y.; Yang, Z.; Zhao, Y.; Yang, X.; Gong, T.; Li, C. Femtosecond laser micromachining in combination with ICP etching for 4H-SiC pressure sensor membranes. *Ceram. Int.* **2021**, *47*, 6397–6408. [[CrossRef](#)]

124. Xu, X.; Liu, X.; Wu, J.; Zhang, C.; Zhang, Q.; Tian, K. Preparation of mullite whisker reinforced SiC membrane supports with high gas permeability. *Ceram. Int.* **2021**, *47*, 8150–8160. [[CrossRef](#)]
125. Luo, Z.-Y.; Han, W.; Liu, K.-Q.; Ao, W.-Q.; Si, K.-K. Influence of bonding phases on properties of in-situ bonded porous SiC membrane supports. *Ceram. Int.* **2020**, *46*, 8536–8542. [[CrossRef](#)]
126. Liu, J.; Zhu, C.; Liang, W.; Li, Y.; Bai, H.; Guo, Q.; Wang, C. Experimental investigation on micro-scale phase change material based on sodium acetate trihydrate for thermal storage. *Sol. Energy* **2019**, *193*, 413–421. [[CrossRef](#)]
127. Bukhari, S.Z.A.; Ha, J.-H.; Lee, J.; Song, I.-H. Oxidation-bonded SiC membrane for microfiltration. *J. Eur. Ceram. Soc.* **2018**, *38*, 1711–1719. [[CrossRef](#)]
128. Wei, W.; Zhang, W.; Jiang, Q.; Xu, P.; Zhong, Z.; Zhang, F.; Xing, W. Preparation of non-oxide SiC membrane for gas purification by spray coating. *J. Membr. Sci.* **2017**, *540*, 381–390. [[CrossRef](#)]
129. Chung, G.-S.; Jeong, J.-M. Fabrication of micro heaters on polycrystalline 3C-SiC suspended membranes for gas sensors and their characteristics. *Microelectron. Eng.* **2010**, *87*, 2348–2352. [[CrossRef](#)]
130. Bukhari, S.Z.A.; Ha, J.-H.; Lee, J.; Song, I.-H. Effect of different heat treatments on oxidation-bonded SiC membrane for water filtration. *Ceram. Int.* **2018**, *44*, 14251–14257. [[CrossRef](#)]
131. Wang, Y.; Jiang, Q.; Jing, W.; Zhong, Z.; Xing, W. Pore structure and surface property design of silicon carbide membrane for water-in-oil emulsification. *J. Membr. Sci.* **2022**, *648*, 120347. [[CrossRef](#)]
132. Wang, W.; Zhang, B.; Shi, Y.; Zhou, J.; Wang, R.; Zeng, N. Improved Chemical Mechanical Polishing Performance in 4H-SiC Substrate by Combining Novel Mixed Abrasive Slurry and Photocatalytic Effect. *Appl. Surf. Sci.* **2022**, *575*, 151676. [[CrossRef](#)]
133. Rico-Santacruz, M.; García-Muñoz, P.; Keller, V.; Batail, N.; Pham, C.; Robert, D.; Keller, N. Alveolar TiO₂-β-SiC photocatalytic composite foams with tunable properties for water treatment. *Catal. Today* **2019**, *328*, 235–242. [[CrossRef](#)]
134. Gao, Z.; Abbasian, J.; Arastoopour, H. Modeling and numerical simulation of concentrated solar energy storage in a packed bed of silicon carbide particles. *Ind. Eng. Chem. Res.* **2021**, *60*, 16498–16508. [[CrossRef](#)]
135. Xie, H.Q.; Cai, X.Y.; Cui, K.Y.; Yi, X.B.; Lu, J.L.; Fan, Z.Q. High-performance monolayer or bilayer SiC short channel transistors with metallic 1T-phase MoS₂ contact. *Phys. Lett. A* **2022**, *436*, 128070. [[CrossRef](#)]
136. He, Z.; Yu, C.; Liu, Q.; Song, X.; Gao, X.; Guo, J.; Zhou, C.; Cai, S.; Feng, Z. High temperature RF performances of epitaxial bilayer graphene field-effect transistors on SiC substrate. *Carbon* **2020**, *164*, 435–441. [[CrossRef](#)]
137. Jia, H.; Zhang, Y.; Wang, H.; Zhu, S.; Wang, X.; Shen, Y.; Yang, Y. Improved 4H-SiC MESFET with bulgy channel. *Micro Nanostruct.* **2022**, *166*, 207222. [[CrossRef](#)]
138. Jia, H.; Zhang, Y.; Zhu, S.; Wang, H.; Wang, X.; Liang, H.; Yang, Y. A novel 4H-SiC MESFET with P-type doping zone and recessed buffer layer. *Mater. Sci. Semicond. Process.* **2022**, *144*, 106615. [[CrossRef](#)]
139. Baierhofer, D.; Thomas, B.; Staiger, F.; Marchetti, B.; Förster, C.; Erlbacher, T. Defect reduction in SiC epilayers by different substrate cleaning methods. *Mater. Sci. Semicond. Process.* **2021**, *140*, 106414. [[CrossRef](#)]
140. Yang, X.; Yang, X.; Kawai, K.; Arima, K.; Yamamura, K. Novel SiC wafer manufacturing process employing three-step slurryless electrochemical mechanical polishing. *J. Manuf. Process.* **2021**, *70*, 350–360. [[CrossRef](#)]
141. Liu, Z.; Cai, Y.; Tu, R.; Xu, Q.; Hu, M.; Wang, C.; Sun, Q.; Li, B.-W.; Zhang, S.; Wang, C.; et al. Laser CVD growth of graphene/SiC/Si nano-matrix heterostructure with improved electrochemical capacitance and cycle stability. *Carbon* **2021**, *175*, 377–386. [[CrossRef](#)]
142. Yang, C.; Wei, B.; He, K.; Xu, P.; Xie, X.; Tong, K.; Zeng, C.; Wang, Y.; Wang, X.; Liu, J.; et al. Simple and rapid conversion of silicon carbide to nanodiamonds at ambient pressure. *J. Mater. Sci. Technol.* **2021**, *94*, 230–238. [[CrossRef](#)]
143. Chen, Y.; Wang, X.; Deng, C.; Yu, C.; Ding, J.; Zhu, H. Controllable synthesis of Si@SiC plate@Si₃N₄ whisker with core-shell structure and their electrochemical performances. *Powder Technol.* **2021**, *377*, 324–335. [[CrossRef](#)]
144. Sri Maha Vishnu, D.; Sure, J.; Kim, H.K.; Kumar, R.V.; Schwandt, C. Solid state electrochemically synthesised β-SiC nanowires as the anode material in lithium ion batteries. *Energy Storage Mater.* **2020**, *26*, 234–241. [[CrossRef](#)]
145. Zhang, Z.; Li, H. Sequential-template synthesis of hollowed carbon polyhedron@SiC@Si for lithium-ion battery with high capacity and electrochemical stability. *Appl. Surf. Sci.* **2020**, *514*, 145920. [[CrossRef](#)]
146. Singla, S.; Kang, A.S.; Sidhu, T. Characterization and electrochemical corrosion behaviour of FSPed WE43/nano-SiC surface composite. *Mater. Today Proc.* **2020**, *26*, 3138–3144. [[CrossRef](#)]
147. Zhuo, L.; Zhang, Q.; Zhang, Y.; Zhao, Z.; Liang, S.; Chen, Q.; Wang, H.; Zhang, J. Tailoring the microstructure and properties of tungsten-copper composites by minor addition of SiC particles for nuclear fusion reactor application. *J. Nucl. Mater.* **2020**, *538*, 152220. [[CrossRef](#)]
148. Istomina, E.I.; Istomin, P.V.; Nadutkin, A.V.; Grass, V.E.; Lysenkov, A.S. Synthesis of C/SiC core-shell fibres through siliconization of carbon fibres with SiO gas in semi-closed reactor. *Ceram. Int.* **2021**, *47*, 22587–22593. [[CrossRef](#)]
149. Seshadri, A.; Phillips, B.; Shirvan, K. Impact of nuclear environment on hydrothermal corrosion and silica transport for CVD SiC in light water reactors. *J. Nucl. Mater.* **2021**, *556*, 153155. [[CrossRef](#)]
150. Jarman, J.D.; Fahrenholtz, W.G.; Hilmas, G.E.; Watts, J.L.; King, D.S. Characterization of fusion welded ceramics in the SiC-ZrB₂-ZrC system. *J. Eur. Ceram. Soc.* **2021**, *41*, 2255–2262. [[CrossRef](#)]
151. Jarman, J.D.; Fahrenholtz, W.G.; Hilmas, G.E.; Watts, J.L.; King, D.S. Mechanical properties of fusion welded ceramics in the SiC-ZrB₂ and SiC-ZrB₂-ZrC systems. *J. Eur. Ceram. Soc.* **2022**, *42*, 2107–2117. [[CrossRef](#)]

152. Lv, X.; Ye, F.; Cheng, L.; Zhang, L. 3D printing “wire-on-sphere” hierarchical SiC nanowires/SiC whiskers foam for efficient high-temperature electromagnetic wave absorption. *J. Mater. Sci.* **2022**, *109*, 94–104. [[CrossRef](#)]
153. Wang, Y.; Liu, H.; Mei, D.; Wu, Q.; Zhou, H. A novel thermally autonomous methanol steam reforming microreactor using SiC honeycomb ceramic as catalyst support for hydrogen production. *Int. J. Hydrogen Energy* **2021**, *46*, 25878–25892. [[CrossRef](#)]
154. Xiong, C.; Li, T.; Zhao, T.; Khan, M.; Wang, J.; Ji, X.; Li, H.; Liu, W.; Shang, Y. Preparation of C/C–SiC composite by low temperature compression molding–liquid silicon infiltration and its application in automobile brake. *Ceram. Int.* **2016**, *42*, 1057–1062. [[CrossRef](#)]
155. Zhao, S.; Zhang, X.; Zhong, W.; Wen, Y.; Yan, Q. The wet braking and recovery behaviors of the P/M pad mated with C/C–SiC disc for high-speed trains. *Wear* **2021**, *468–469*, 203609. [[CrossRef](#)]
156. Zhao, S.; Yan, Q.; Peng, T.; Zhang, X.; Wen, Y. The braking behaviors of Cu-Based powder metallurgy brake pads mated with C/C–SiC disk for high-speed train. *Wear* **2020**, *448–449*, 203237. [[CrossRef](#)]
157. Jiang, L.; Jiang, Y.; Yu, L.; Yang, H.; Li, Z.; Ding, Y.; Fu, G. Fabrication, microstructure, friction and wear properties of SiC₃D/Al brake disc–graphite/SiC pad tribo-couple for high-speed train. *T. Nonferr. Metal. Soc.* **2019**, *29*, 1889–1902. [[CrossRef](#)]

Disclaimer/Publisher’s Note: The statements, opinions and data contained in all publications are solely those of the individual author(s) and contributor(s) and not of MDPI and/or the editor(s). MDPI and/or the editor(s) disclaim responsibility for any injury to people or property resulting from any ideas, methods, instructions or products referred to in the content.